JGR Atmospheres

RESEARCH ARTICLE
10.1029/2023JD038865

Insights Into NO_x and HONO Chemistry in the Tropical Marine Boundary Layer at Cape Verde During the MarParCloud Campaign

Ying Jiang[1,2], Erik H. Hoffmann[1], Andreas Tilgner[1], Marvel B. E. Aiyuk[1], Simone T. Andersen[3], Liang Wen[1,4], Manuela van Pinxteren[1], Hengqing Shen[2], Likun Xue[2], Wenxing Wang[2], and Hartmut Herrmann[1,5]

[1]Atmospheric Chemistry Department (ACD), Leibniz Institute for Tropospheric Research (TROPOS), Leipzig, Germany, [2]Environment Research Institute, Shandong University, Qingdao, China, [3]Max-Planck-Institut für Chemie (MPIC), Mainz, Germany, [4]Now at Chinese Research Academy of Environmental Sciences, Beijing, China, [5]School of Environmental Science and Engineering, Shandong University, Qingdao, China

Abstract Chemical processing of reactive nitrogen species, especially of NO_x (= NO + NO_2) and nitrous acid (HONO), determines the photochemical ozone production and oxidation capacity in the troposphere. However, sources of HONO and NO_x in the remote marine atmosphere are still poorly understood. In this work, the multiphase chemistry mechanism CAPRAM in the model framework SPACCIM was used to study HONO formation at Cape Verde (CVAO) in October 2017, adopted with the input of current parameterizations for various HONO sources. Three simulations were performed that adequately reproduced ambient HONO levels and its diurnal pattern. The model performance for NO_x and O_3 improves significantly when considering dust-surface-photocatalytic conversions of reactive nitrogen compounds with high correlation coefficients up to 0.93, 0.56, and 0.89 for NO, NO_2, and O_3, respectively. Photocatalytic conversion of the adsorbed HNO_3 on dust is modeled to be the predominant contributor for daytime HONO at CVAO, that is, accounting for about 62% of the chemical formation rate at noontime. In contrast, the ocean-surface-mediated conversion of NO_2 to HONO and other discussed pathways are less important. The average OH levels at midday (9:00–16:00) modeled for cluster trajectory 1, 2, and 3 are 5.2, 5.1, and 5.2 × 10^6 molecules cm^{-3}, respectively. Main OH formation is driven by O_3 photolysis with a contribution of 74.6% to the total source rate, while HONO photolysis is negligible (~1.8%). In summary, this study highlights the key role of dust aerosols for HONO formation and NO_x cycling at CVAO and possibly in other dust-affected regions, urgently calling for further investigations using field and model studies.

Plain Language Summary Chemical processing of NO_x (= NO + NO_2) and nitrous acid (HONO) is important for the tropospheric O_3 budget and oxidation capacity. However, the sources of HONO and cycling of NO_x in the remote marine atmosphere are still poorly explored. A detailed multiphase chemistry model simulation showed a better performance of HONO, NO_x and O_3 when considering dust-surface-photocatalytic conversions of reactive nitrogen compounds, especially the photocatalytic conversion of the adsorbed HNO_3 on dust. The simulations demonstrated that OH formation is mainly driven by the O_3 photolysis, while HONO photolysis is a negligible OH radical source due to its low concentration levels at Cape Verde. The study highlights the key role of dust aerosols for HONO and NO_x chemistry in the remote marine boundary layer.

Key Points:

- The sources of HONO and NO_x at Cape Verde are well modeled with CAPRAM
- Photocatalytic conversion of adsorbed HNO_3 on dust is the predominant contributor for daytime HONO
- Photolysis of O_3 is the prevailing source of OH radical at Cape Verde, while HONO photolysis is a negligible OH radical source

Supporting Information:

Supporting Information may be found in the online version of this article.

Correspondence to:

L. Xue and H. Herrmann,
xuelikun@sdu.edu.cn;
herrmann@tropos.de

Citation:

Jiang, Y., Hoffmann, E. H., Tilgner, A., Aiyuk, M. B. E., Andersen, S. T., Wen, L., et al. (2023). Insights into NO_x and HONO chemistry in the tropical marine boundary layer at Cape Verde during the MarParCloud campaign. *Journal of Geophysical Research: Atmospheres*, *128*, e2023JD038865. https://doi.org/10.1029/2023JD038865

Received 10 MAR 2023
Accepted 7 AUG 2023

Author Contributions:

Conceptualization: Likun Xue, Hartmut Herrmann
Formal analysis: Ying Jiang, Erik H. Hoffmann, Andreas Tilgner, Marvel B. E. Aiyuk, Simone T. Andersen, Liang Wen, Manuela van Pinxteren, Hengqing Shen, Likun Xue, Wenxing Wang, Hartmut Herrmann
Investigation: Ying Jiang, Erik H. Hoffmann, Andreas Tilgner

1. Motivation and Introduction

The chemical processing of reactive nitrogen species (RNS), especially NO_x (= NO + NO_2) and nitrous acid (HONO), is very important for the atmospheric oxidation capacity due to the photochemical production of ozone (O_3) as well as the OH radical in the troposphere (Alicke et al., 2003; Sherwen et al., 2016). After sunrise, the photolysis of HONO can be a key formation pathway for OH radicals in the ambient continental atmosphere (Gu et al., 2020; Li et al., 2018). In addition, effective cycling between the NO_x and HO_x system is established due to the reaction between NO and HO_2. This reaction is important for OH recycling after the initial formation of OH from the O_3 photolysis under higher NO_x conditions (Stone et al., 2012; Whalley et al., 2010). Recent field measurements also indicate the importance of HONO photolysis for the OH radical budget in the coastal atmosphere in Qingdao, China (Yang et al., 2021). However, robust evidence for the involvement of HONO in OH formation under pristine marine conditions is still lacking. A quantitative understanding of the chemical

Methodology: Ying Jiang, Erik H. Hoffmann, Andreas Tilgner, Hartmut Herrmann
Resources: Simone T. Andersen, Liang Wen, Hartmut Herrmann
Supervision: Likun Xue, Hartmut Herrmann
Validation: Ying Jiang, Erik H. Hoffmann, Andreas Tilgner
Writing – original draft: Ying Jiang, Erik H. Hoffmann, Andreas Tilgner, Manuela van Pinxteren, Hartmut Herrmann
Writing – review & editing: Ying Jiang, Erik H. Hoffmann, Andreas Tilgner, Marvel B. E. Aiyuk, Simone T. Andersen, Liang Wen, Manuela van Pinxteren, Hengqing Shen, Likun Xue, Wenxing Wang, Hartmut Herrmann

processing of NO_x and HONO in the marine boundary layer (MBL) is important to understand local, regional and global ozone budgets which are connected to the wider atmospheric oxidation capacity. As a consequence, it is necessary to further evaluate the contribution of HONO photolysis on the OH level in the MBL due to the sparse HONO observations.

In comparison to the sink processes, that is, primarily photolysis, which are relatively well understood, the sources of ambient HONO in the troposphere, especially during daytime, are still being extensively investigated and discussed. A large missing HONO source has inevitably been found in different field observations and simulations over the past decades when considering current known HONO formation mechanisms (e.g., direct vehicular emissions, gas-phase reactions of NO and OH, and soil emission) (Gu et al., 2020; Jiang et al., 2020; Liu et al., 2019; Su et al., 2011; Xue et al., 2022; Yang et al., 2021). However, direct vehicular emissions and soil/ground emissions are unimportant at the CVAO site (van Pinxteren et al., 2020). Until recently, various heterogeneous mechanisms have been proposed to explain the observed HONO concentration involving various surfaces (i.e., ground, aerosol/dust, forest canopy, soil, and ocean) (Spataro & Ianniello, 2014; Wong et al., 2011; Yang et al., 2021). Among these, heterogeneous photosensitized/catalyzed NO_2 conversions to HONO enhanced by solid/aqueous organics, soot, or titanium dioxide (TiO_2) on different types of surfaces have widely been recognized as contributing to the observed daytime HONO levels, especially in urban regions, as described by the following stoichiometry (Reaction R1) (Liu et al., 2014; Spataro & Ianniello, 2014; VandenBoer et al., 2013; Wong et al., 2012).

$$2\,NO_{2(g)} + H_2O_{(surface)} \rightarrow HONO_{(g)} + HNO_{3\,(surface)} \quad (R1)$$

Other heterogeneous reactions, such as the reaction of NO (a) with NO_2 and water or (b) with HNO_3 and water, appear to play only a minor role in HONO formation (Calvert et al., 1994; Park & Lee, 1988; Saliba et al., 2001). Besides this, ammonia photooxidation on aerosol with TiO_2/SiO_2 produces NO, which subsequently could also enhance HONO formation (Kebede, Scharko, et al., 2013; Kebede, Varner, et al., 2013). Recent model simulations suggest ammonia oxidation by OH may have an impact on atmospheric chemistry in remote NO_x-limited regions by serving as a small but relatively significant source of NO (Pai et al., 2021) and thus might affect HONO formation. The photolysis of the nitric acid (HNO_3) or particulate nitrate (pNO_3^-) deposited on various surfaces such as ground, aerosol, forest canopy, and snowpack, enhanced by the presence of organics/halogens, has been suggested to be important based on the field measurements in remote continental/marine areas and laboratory studies (Andersen et al., 2023; Reed et al., 2017; Wang et al., 2020; Ye et al., 2016, Ye, Heard, et al., 2017, Ye, Zhang, et al., 2017; Zhang et al., 2020). A recent field campaign has highlighted the effect of evaporation from dew droplets to explain high sunrise HONO levels (Ren et al., 2020). Nevertheless, this process can be neglected in marine areas.

The available observation and simulation studies of HONO are mainly conducted in polluted environments, with limited efforts performed in the pristine MBL, hindering a better understanding of trends, chemical processes and impacts of tropospheric HONO on a global scale. Accordingly, the relative significance of different surfaces (ocean-surfaces versus aerosol/dust surfaces) on ambient HONO in the MBL is still under debate (see e.g., Crilley et al., 2021). Moreover, the potential role of the oceans and aerosols on ambient HONO showed a different spatial distribution based on very limited numbers of measurements within the MBL (Crilley et al., 2021; Cui et al., 2019; Reed et al., 2017). Considering the large surface area of the oceans, it could be a possible interface for converting NO_2 to HONO. Accordingly, Zha et al. (2014) observed large conversion rates of NO_2 to HONO in continental air masses transported over the South China Sea, which was attributed to the sea surface. A similar finding was observed at Tuoji island in the eastern Bohai Sea, China (Wen et al., 2019) and Qingdao, a coastal site by the Huanghai Sea, China (Yang et al., 2021). Later, a missing daytime HONO source from a shipboard-based HONO measurement from an area with heavy shipping traffic (East China Sea) was related to a light-induced HONO source from NO_2 on the sea surface and pNO_3^- (Cui et al., 2019). All of these results provided certain indirect evidence for the importance of the oceans, especially the efficient sea surface microlayer (SML) with its high abundance of organics and high surface density. However, model results of an aircraft HONO measurement over the North Atlantic Ocean indicated that a pNO_3-NO_x cycle occurring in or on aerosols is capable of reaching the observed midday levels of HONO and NO_x in the MBL (Ye et al., 2016). Earlier, Ndour et al. (2008, 2009); found that mineral dust containing TiO_2/SiO_2 could provide an efficient surface for nitrogen species to be absorbed and converted. Reactions on dust aerosols could produce NO_x deriving from photodissociation of pNO_3^- due to the photocatalytic properties of TiO_2. However, there is significant uncertainty on the role

of HNO_3/pNO_3^- photolysis on HONO formation. Current studies (see e.g., Andersen et al., 2023 and references therein) suggest that pNO_3^- concentration and its photolysis play a key role, but agree with measurements that unfortunately can only be obtained by increasing the HONO formation rates unrealistically up to levels which have limited foundation in either gas or aqueous phase direct laboratory investigations. As outlined by Reed et al. (2017), who investigated NO_x cycling at Cape Verde, this high rate "conceptually it includes any additional surface production of HONO and NO_2." Overall, the relative importance of the oceans and aerosols within the marine influenced troposphere is being very active discussed and needs to be further studied with clear experimental observations together with extended near-explicit multiphase chemistry process models.

To explore the diurnal behavior and chemical processes responsible for the HONO and NO_x cycling in pristine MBL, time series measurements of HONO, NO_x, aerosols and other related parameters were performed at the Cape Verde Atmospheric Observatory (CVAO) between 2 October and 11 October 2017 as the MarParCloud project led by TROPOS-ACD which aimed to gain deeper insights into the processes and the impact of marine organic matter (OM) acting as ice-nucleating particles (INPs) and cloud condensation nuclei (CCN) (van Pinxteren et al., 2020). In the present study, the measured HONO and NO_x at CVAO were explored using the advanced multiphase model SPACCIM (Wolke et al., 2005) coupled with the comprehensive multiphase chemistry mechanism system MCMv3.2/CAPRAM4.0 (Bräuer et al., 2019) and with distinct reaction modules to describe marine related multiphase chemistry of dimethyl sulfide (DMS) and reactive halogen species (RHS) (Hoffmann et al., 2016). The present study aims to understand the contribution of the different production mechanisms for HONO and NO_x diel patterns especially during daytime as well as the impact of HONO photolysis on the OH levels under pristine MBL conditions.

2. Methods and Mechanism Implementation

2.1. Instrumentation

The CVAO is a background remote marine site on the island of São Vincente situated in the tropical North Atlantic upwelling region off the coast of West Africa (16.864°N, 24.868°W) (Figure S1 in Supporting Information S1). The site is located directly at the shoreline at the northeastern tip of the island of São Vicente at 10 m a.s.l., which has no obvious major coastal features such as extensive shallows or large seaweed beds. Thus, it could not provide an effective ground source (i.e., NO_2 heterogeneous reaction on grounds) for HONO and NO_x formation. This sampling site has been widely used to investigate the background remote MBL in the past decade (Carpenter et al., 2010; Weinzierl et al., 2011). In general, there are some local residential emissions, but the trade winds from the northeast (approaching from the ocean) are stable and prevalent at the site (Figure S2 in Supporting Information S1). Thus, the impact of local anthropogenic emissions is negligible. However, it is likely that ship emissions as well as anthropogenic emissions from Dakar and Nouakchott can influence the level of RNS (Carpenter et al., 2010). The coast of West Africa is situated ~900 km to the east, and CVAO is located on the typical transport pathway of Saharan dust from North Africa to the North Atlantic. It therefore often suffers from dust pollution from the Sahara Desert. A more detailed description of the station and its equipment can be found in Carpenter et al. (2010), Fomba et al. (2014), and van Pinxteren et al. (2020).

A wide range of chemical, physical, and meteorological parameters were measured in real time during the MarParCloud campaign. Details and other related issues are given in the overview paper by van Pinxteren et al. (2020). Here, only a brief description of the measurement techniques for the species of interest in the present study is given. HONO was detected by a long-path absorption photometer (LOPAP-03, QUMA GmbH, Germany) operated between 2 October and 11 October 2017. A detailed description of the LOPAP instrument has been provided by Heland et al. (2001). During the observations, the calibration process was conducted every 4 days using 1000 mg/L nitrite standard solutions to inspect the sensitivity of the detector. However, it has to be noted that the small drift of the baseline was corrected without any ambient air or the ultrapure nitrogen every 12 hr due to issues during the calibration. It may cause the measured HONO value at CVAO to be higher than its "true" concentration. Therefore, detailed information of the HONO data and comparison with previous measurements were performed and are discussed in Section 3.1. NO and NO_2 were measured using NO chemiluminescent detector (CLD), where NO is oxidized by excess O_3 into excited NO_2 in the reaction volume (241 mL, aluminum with gold coating; Ridley & Grahek, 1990) as described by Andersen et al. (2021). O_3 was measured by a UV absorption instrument (Model 49i Thermo Scientific). VOCs and OVOCs were measured by a dual channel gas chromatograph equipped with flame ionization detection (Agilent 7890-A). Particle number size distribution (PNSD)

data from the SMPS and APS were used to calculate the surface area of particles. High volume PM_1, PM_{10} and total suspended particulate (TSP) were measured by a commercial instrument (Digitel, Riemer, Germany) and filter samplers (Sierra Anderson, USA), respectively. Furthermore, the aerosol composition data from these samplers were used to evaluate the model predictions. Meteorological data including temperature, relative humidity (RH), pressure, wind speed and direction were measured using a meteorological station equipped with various sensors (Campbell Scientific Ltd., UK). All of these techniques have been successfully applied in previous studies, and the detailed information of operation, quality assurance, and quality control procedures can be found in van Pinxteren et al. (2020).

2.2. Categorization of Airmass Advection by Backward Trajectory Analysis

For the period of 2 October to 11 October 2017, 72 hr backward trajectories of the arriving air masses for every hour were explored and further classified into three clusters to investigate the origins and movement pathways of air masses sampled at CVAO. The hourly three-dimensional backward trajectories with a final height of 250 m above ground level (AGL) at CVAO were computed by the Hybrid Single Particle Lagrangian Integrated Trajectory model (HYSPLIT Model, version 4.8, 2010, from R. R. Draxler and G. D. Rolph, http://ready.arl.noaa.gov/HYSPLIT.php) (HYSPLIT, 2019), equipped with the Global Data Assimilation System (GDAS) meteorological data and then applied to the cluster analysis (Figure S3 in Supporting Information S1). Three obtained clusters are described as follows: NE (Cluster 1), air masses coming from the local northeast direction with the largest proportion of 56% of total backward trajectories; CA (Cluster 2), air masses originating from the regions near the coastline of West Africa, accounting for 23% of total backward trajectories; AM (Cluster 3), air masses originating over remote Atlantic Ocean and transported quickly over the tropical MBL.

2.3. SPACCIM Model Configurations and Inputs

The multiphase chemistry simulations along every cluster were performed with the air-parcel model framework SPACCIM (Spectral Aerosol Cloud Chemistry Interaction Model) (Wolke et al., 2005), in which multiphase chemistry is described by coupling the near-explicit gas-phase mechanism MCMv3.2 (MCMv3.2, 2014) with the aqueous-phase mechanism CAPRAM4.0 (Bräuer et al., 2019). The CAPRAM (CAPRAM, 2021) mechanism has often been successfully applied to understand field measurements (Guo et al., 2014; Ye et al., 2021; Zhu et al., 2020). The description of multiphase chemistry of RHS and DMS is realized by coupling the CAPRAM–HM3.0 (Hoffmann et al., 2019) and CAPRAM–DM1.0 (Hoffmann et al., 2016), respectively. Additionally, a chemistry module describing the oxidation of aromatic compounds in the aqueous phase, the CAPRAM–AM1.0 (Hoffmann et al., 2018), has been coupled to represent possible interactions of organic anthropogenic pollutants with NO_x affecting aqueous HONO formation. A detailed description of the SPACCIM model framework is given in Wolke et al. (2005) and Sehili et al. (2005). The HONO mechanism implemented in MCM3.2/CAPRAM4.0 includes the gas reaction of NO and OH (in MCM mechanisms), the HONO phase transfer process and aqueous-phase reactions as well as relatively complete sinks (i.e., HONO photolysis, the reaction of HONO and OH in the gas phase and other HONO loss reactions in the aqueous phase (Ervens et al., 2003)). All scenarios were initialized with meteorological conditions, emission values, initial concentrations, and deposition rates in the MBL, respectively. The emission values are the sum of anthropogenic and marine emission values. Anthropogenic emissions are taken from the Atmospheric Chemistry and Climate Model Intercomparison Project (ACCMIP; Lamarque et al., 2010) from 2017 and derived for the specific cluster. Marine emissions are derived from a literature survey, except for DMS, for which a monthly mean for October 2017 was used for each cluster. The DMS emission was calculated online in a previous study (Hoffmann et al., 2021). The Lagrangian-type parcel model is initialized by meteorological conditions and chemical compositional data (e.g., emission rates and initial gas-phase concentrations of compounds such as NO_x, O_3, CO, VOCs, OVOCs, etc. (see data given in Tables S1 and S2 in Supporting Information S1). With this input data, the model simulates the chemistry along the model trajectory by means of a detailed chemical multiphase mechanism. However, as stated in the text, some meteorological condition parameters need to be adjusted to the local ambient conditions. For example, all photolysis rates considered in the model were scaled using the measured J_{HONO} at CVAO in order to avoid any overestimation of photolysis processes. Initial and deposition values that were not measured are used from the pristine marine scenario setup of CAPRAM (Hoffmann et al., 2016). The detailed emission data, initial data, and deposition rates are summarized in Tables S1–S3 in Supporting Information S1, respectively.

Table 1
Parameterization of HONO Sources Added to the "BaseCase" Mechanism and Sensitivity Scenario Setting

Nr.	Scenario setting	Simulation identifier	HONO mechanisms
1	MCM	"MCM"	Only gas-phase reaction
2	MCM/CAPRAM	"BaseCase"	Gas-phase reaction; HONO phase transfer; Related aqueous reactions
3	MCM/CAPRAM + NO_2 reacted with organics in aerosols	"BaseCase + NO_2_org"	BaseCase + see Table S5 in Supporting Information S1
4	MCM/CAPRAM + NO_2 deposition on the sea surface then converted to HONO	"BaseCase + NO_2_depo"	BaseCase + see Table S5 in Supporting Information S1
5	MCM/CAPRAM + NH_3 oxidation	"BaseCase + NH_3"	BaseCase + see Table S5 in Supporting Information S1
6	MCM/CAPRAM + Nitrogen species uptake on dust	"BaseCase + Nitro"	BaseCase + see Table S5 in Supporting Information S1
7	MCM/CAPRAM + Nitrogen species uptake on dust but without HNO_3 photolysis	"BaseCase + Nitro_woHNO_3"	BaseCase + see Table S5 in Supporting Information S1
8	MCM/CAPRAM + Nitrogen species uptake on dust; but without I_2/Br_2 emission data	"BaseCase + Nitro_woHalogens"	BaseCase + see Table S5 in Supporting Information S1

All simulations were carried out for 72 hr (3 days) starting at 00:00, using the first 24 hr (1 day) as a spin-up time to allow the intermediates to reach ambient levels. The last day of the simulations was used for comparison with the measured average diurnal variations of HONO, NO_x as well as O_3 during the three different clusters to assess the performance of the model simulations and, thus, its ability to accurately describe the atmospheric oxidation capacity.

2.4. Parameterization of Different HONO Sources

The default MCM/CAPRAM mechanism has two HONO formation pathways, including the homogeneous gas-phase reaction of NO and OH in the MCM part and the phase transfer process of HONO between gas and aqueous phase. The latter can act as a source for the gas-phase when HONO is produced by aqueous-phase processes. The detailed aqueous-phase HONO mechanisms already implemented in CAPRAM4.0 and CAPRAM-AM1.0 can be found in Ervens et al. (2003) and Hoffmann et al. (2018). Within the present study, besides the default MCM/CAPRAM mechanism, only a simulation with the MCMv3.2 has been performed. Furthermore, additional HONO sources were incorporated into the model system to perform different sensitivity studies. The different additional HONO formation pathways considered in the sensitivity investigations are outlined below. The detailed scenario settings of each sensitivity study including their abbreviation is given in Table 1.

2.4.1. Ocean-Surface-Mediated Conversion of NO_2 to HONO

As discussed in Section 1, the SML may act as a reactive medium for HONO formation reactions. Many previous studies reported that the NO_2-to-HONO conversion rate on the oceans was much higher than that coming from continental regions (Wen et al., 2019; Yang et al., 2021; Zha et al., 2014). However, Crilley et al. (2021) indicated that the NO_2-to-HONO conversion rate on the oceans (C_{HONO}) with an upper limit of 0.0011 hr^{-1} at CVAO was much lower than that at the coastal site of Hok Tsui, China (0.033 hr^{-1}) (Zha et al., 2014). In this sensitivity simulation, the SML-related NO_2-to-HONO conversion is simplified as the NO_2 molecules reached the sea surface via dry deposition (v_d = 0.29 cm s^{-1}) (Loughner et al., 2016) and the assumption is made that all of the deposited NO_2 would be converted to HONO and released to the atmosphere immediately, as shown in the following conceptual Reaction R2 and Table S5 in Supporting Information S1. Still, the contribution of this pathway to the HONO formation in marine boundary layer remains controversial. The contribution from this approach for HONO formation may significantly depend on the deposition loss rate of NO_2, but is also limited toward the concentration of organics in the SML, which is presented in Figure S4 in Supporting Information S1.

$$NO_{2(g)} \rightarrow HONO_{(g)} \quad \text{(R2)}$$

2.4.2. Reaction of NO_2 With Organics in Deliquesced Aerosol Particles

HONO formation from reactions of NO_2 on organic surfaces such as aromatic hydrocarbons and humic acids have been proposed for dark and light conditions (George et al., 2005; Stemmler et al., 2006). In this study, the reaction of aqueous NO_2 with organic compounds whose concentrations are modeled to be high in simulation "BaseCase" in the MBL (HULIS, methane sulfinate, methane sulfonate and formate) was added to evaluate the importance of this pathway, as shown in the following conceptual Reaction R3. The reaction rate coefficient has been assumed to be 1×10^7 L mol^{-1} s^{-1} for the dissociated form, in line with measured data (Alfassi et al., 1986; Forni et al., 1986). The detailed reactions of this pathway are listed in Table S5 in Supporting Information S1:

$$NO_{2(aq)} + \text{organics} \rightarrow NO_2^- + \text{others} \quad \text{(R3)}$$

2.4.3. NH_3 Oxidation

Ammonia (NH_3) can act as an important reservoir of reactive nitrogen in the atmosphere and has a critical impact on the global nitrogen cycle. Its oxidation by the OH radical can produce NO (Kohlmann & Poppe, 1999) and is indicated to possibly have significant effects on the NO_x level, especially in a remote NO_x-limited environment (Pai et al., 2021). Here, the mechanisms of the gas-phase NH_3 oxidation process reported by Pai et al. (2021) and by Kohlmann and Poppe (1999) were reviewed. The gas-phase reaction pathways were added to the default MCM/CAPRAM mechanism in order to examine the possible impacts of this pathway on NO_x and HONO at CVAO. A detailed description of the implemented gas-phase reactions can be found in Pai et al. (2021).

2.4.4. Photocatalytic Conversions of Reactive Nitrogen Species on Dust Aerosol Surfaces

At certain times of the year (notably in winter), the CVAO islands are heavily affected by dust pollution from the Sahara Desert. The illuminated mineral dust-carrying specific mineral oxides (e.g., TiO_2, ZnO, iron oxides) exhibits photocatalytic or photoreaction properties. Thus, under light conditions, mineral dust can initiate active photochemistry of RNS, possibly serving as important HONO and NO_x sources in a low NO_x environment (Kebede, Scharko, et al., 2013; Kebede, Varner, et al., 2013; Ndour et al., 2009; Ndour et al., 2008). In this study, the uptake coefficients and yields of reactive gas-phase nitrogen species (NO_2, NH_3, NO_3, N_2O_5, HNO_3, and HONO) absorbed on the mineral dust were included. The applied uptake coefficients are given in Table S4 in Supporting Information S1. It is noted that for this reactive uptake the modeled gas-phase concentrations are used, not the modeled aqueous concentrations. The heterogeneous uptake reaction rate coefficients ($k_{\text{het},i}$) of these reactions were calculated using the following equation:

$$k_{\text{het},i} = \frac{\gamma_i}{4} \times S_a \times c_i \quad (1)$$

where γ_i is the uptake coefficient of each nitrogen species i (Table S4 in Supporting Information S1); S_a is the specific surface area of dust during the observation periods (i.e., average value of 215, 160, 165 μm^2 cm^{-3} in Clusters 1, 2, and 3, respectively); c_i is the mean molecular velocity of species i. The reaction rate of gas-phase NO_2 and HNO_3 on dust could be enhanced by titanium dioxides (TiO_2) under sunlight, which means that the calculated reaction rates (k_{NO_2} and k_{NO_3}) are scaled as functions from the solar zenith angle for NO_2 and nitrate photolysis, respectively. The photocatalytic mechanisms of gas-phase NO_2 and HNO_3 on TiO_2-containing mineral dust could proceed as follows (Goldstein et al., 2005; Ndour et al., 2009):

$$\text{Dust}\,(TiO_2) + h\nu \rightarrow h^+_{vb} + e^-_{cb} \quad \text{(R4)}$$

$$NO_3^- + h^+_{vb} \rightarrow NO_3 \quad \text{(R5)}$$

$$NO_3 + h\nu \rightarrow NO + O_2 \quad \text{(R6)}$$

$$NO_3 + h\nu \rightarrow NO_2 + O(^3P) \quad \text{(R7)}$$

$$O_2 + e^-_{cb} \rightarrow O_2^- \quad \text{(R8)}$$

$$NO_2 + O_2^- \rightarrow O_2 + NO_2^- \quad \text{(R9)}$$

$$NO + O_2^- \rightarrow\rightarrow NO_2^- + H_2O_2 - H_2O \quad \text{(R10)}$$

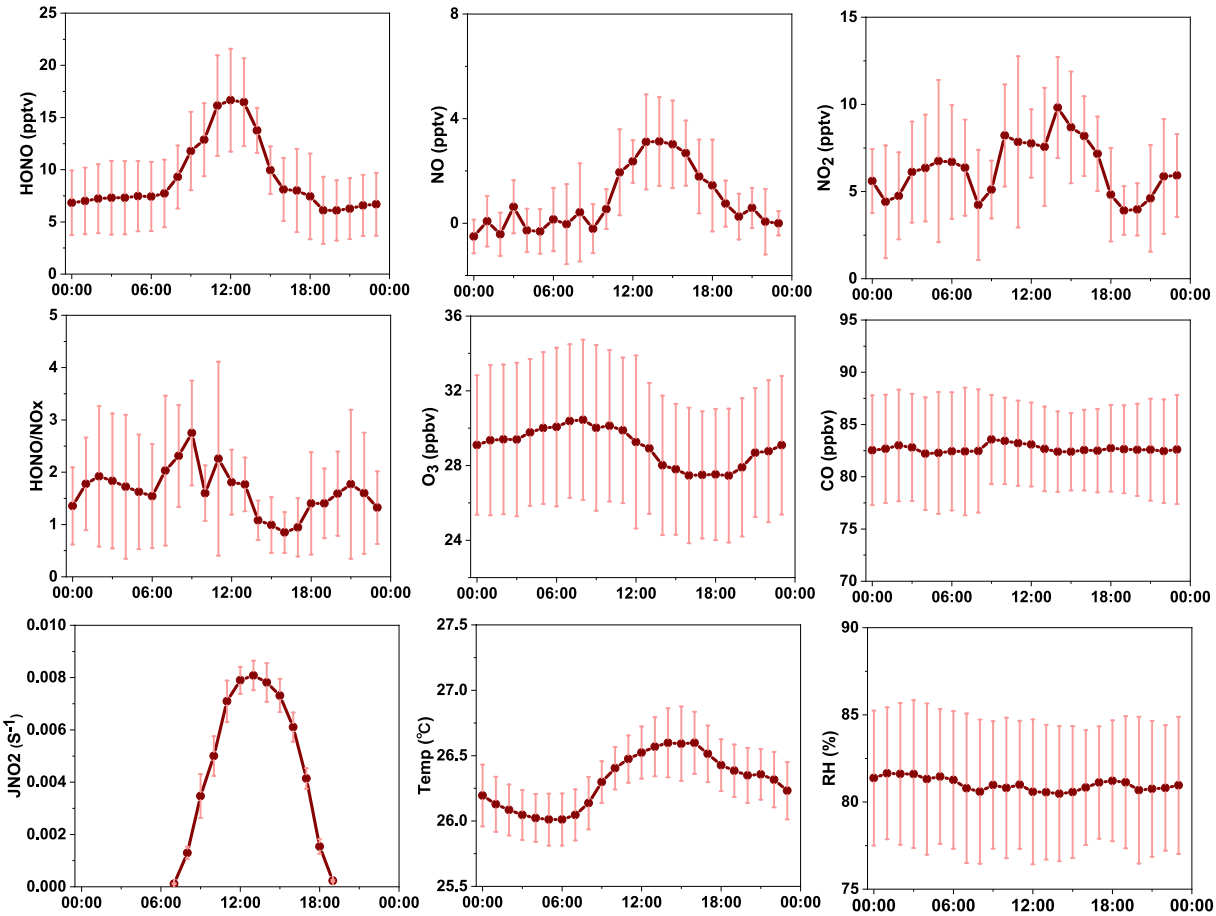

Figure 1. Diurnal variation of HONO and related parameters measured from 2 October to 11 October 2017 at Cape Verde (CVAO) during the MarParCloud campaign. The red lines are the average data of measurement and the pink error lines are the standard deviations.

A critical point for the reactive uptake of gas-phase HNO_3 is the yield of HONO. In accordance with previous studies, a HONO yield of two third is assumed (Ye et al., 2016). The residual yields are NO and NO_2, distributed equally as for the NO_3 photolysis in the aqueous phase. Furthermore, two important factors need to be considered when examining these uptake mechanisms to adjust the uptake rates for mineral dust. One is the content of TiO_2 in mineral dust at CVAO ranging between 0.3 wt% (Salvador et al., 2016) and 1 wt% in Saharan dust (Ndour et al., 2008). The second factor is the effective surface area of ambient mineral dust aerosol, which can be much enhanced over the geometrical surface because of the materials porosity. The detailed description of the impacts of porosity and effective surface area of dust particles can be found in Text S1 in Supporting Information S1. The effective surface area could be much higher than the geometrical surface due to the dust particles being porous and nonspherical, significantly increasing the S_a. Thus, this parameter can be an important factor for the reaction rate of the uptake processes (Tang et al., 2017). Adams et al. (2005) reported that the effective surface area is about 50–80 times that of the geometrical surface. Following this suggestion, a factor of 50 was chosen as an adjustment factor to enhance the abovementioned uptake rates. Finally, the integrated adjustment factor of 15 (calculated by 50×0.3) was used to correct the calculated uptake reaction rates. The detailed reactions and all process parameters used for all considered pathways are given in Table S5 in Supporting Information S1.

3. Results and Discussion

3.1. Overview on Ambient HONO Observations and Related Compounds

The average diurnal variation of HONO, NO, NO_2, HONO/NO_x, and other related parameters at CVAO are shown in Figure 1. The mean diurnal variations of HONO, NO, and NO_2 (a) show a "typical" diel profile at CVAO with a peak (16.7 pptv; 3.1 pptv; 9.8 pptv, respectively) at noontime and (b) keep at a minimum and constant level (~7

pptv; 0.1 pptv; 5.3 pptv; respectively) at night, revealing a strong daytime source of HONO and NO_x. A strong anthropogenic daytime NO_x emission source is ruled out at the CVAO owing to the impacts of prevailing winds and the lower and stable CO concentration. Daytime HONO peaks in concentration profiles were also reported over remote marine, mountain, forest and polar regions (Jiang et al., 2020; Villena et al., 2011; Ye et al., 2016; Zhou et al., 2011). The higher HONO level during MarParCloud was ascribed to the lack of operation of the small drift of the baseline corrected by ultrapure nitrogen. As a consequence, the HONO concentrations used to compare with simulated results was obtained from the HONO measurements in 2015 autumn reported by Reed et al. (2017). The other parameters (e.g., NO, NO_2, O_3, etc.) used in this study were measured during the MarParCloud campaign. The diurnal pattern of HONO in 2015 autumn reported by Reed et al. (2017) was similar with other previously measured results in Ye, Heard, et al. (2017) at CVAO with a noontime peak value of ∼3.7 pptv (see Figure S11 in Supporting Information S1).

There are three reasons for using HONO data in 2015 for a comparison with the model results presented in this study: First, the winds at CVAO were always prevailed by the trades winds traveling from the northeast (ocean) direction, that provided the stable meteorological condition and origins of air masses arriving at CVAO (Carpenter et al., 2010). Second, NO_x and pNO_3^- have been widely recognized as the key precursors for HONO formation in the troposphere. The concentrations of pNO_3^- and NO_x (average of 1.2 μg m^{-3} and 10.4 pptv in the autumn of 2017, respectively) during the MarParCloud campaign are comparable with those reported by Reed et al. (2017) (average of 1 μg m^{-3} and ∼16.5 pptv, respectively). Third, there were three other HONO diel profiles at CVAO reported by Reed et al. (2017), Ye, Heard, et al. (2017), and Andersen et al. (2023), with a comparable peak value of ∼3.7 pptv in the autumn of 2015, ∼5.2 pptv in the summer of 2007, and ∼5.2 pptv in the August of 2019, revealing that the HONO concentration and profile are kept rather stable. Furthermore, the measured diurnal HONO profile during MarParCloud matches with the previous observations. Additionally, we also discussed the uncertainties from the HONO data applied in Reed et al. (2017). The detailed information is given in Text S2 in Supporting Information S1.

3.2. Model Results

3.2.1. Process Sensitivity Studies

Sensitivity simulations with the aforementioned HONO formation pathways have been performed in order to evaluate the relative importance of each one for HONO formation. The sensitivity simulations and their detailed analysis were performed solely for Cluster 1 because of its dominance. The modeled time evolution of the HONO and NO_x concentrations is presented in Figure 2 for all scenarios listed in Table 1. For the HONO and NO_x simulation, the "BaseCase" simulation can reproduce the HONO diurnal pattern with a noontime peak but significantly underestimate the observed concentration levels by two orders of magnitude for both HONO and NO_x. Interestingly, the simulated HONO and NO_x concentrations in simulation "BaseCase" are essentially lower than in simulation "MCM," revealing that the phase transfer process and aqueous mechanisms of HONO and NO_x considerably reduces their gas-phase levels. Furthermore, aqueous-phase chemistry processes can oxidize HONO and NO_x to nitrate, thereby effectively reducing their concentrations. In the simulation "BaseCase + NO_2_depo," the simulated HONO and NO_x only have a slightly higher concentration than in simulation "BaseCase". This indicates that the NO_2 conversion on the active ocean-surface to form gas-phase HONO does not play a decisive role in the ambient HONO and NO_x at CVAO. This is consistent with the results of Crilley et al. (2021), who reported that the contribution of the oceans to HONO production only accounts for around 10% (midday). However, in some coastal regions, the oceans are proposed to be a significant source of ambient HONO, which could be ascribed to the inconsistency in the sea-surface microlayer composition and NO_x pollution (Yang et al., 2021; Zha et al., 2014). In the simulation "BaseCase + NH_3," it is evident that the model fails to obtain the observed HONO and NO_x levels at CVAO (Figure 2), which implies that NH_3 oxidation is a negligible source for HONO and NO_x. What is striking in Figure 2 is the continuous growth of HONO and NO_x at night in the simulation "BaseCase + NO_2_org," while they sharply decline after sunrise in the daytime, which is not consistent with the observations. So, the reactions of NO_2 with organics fail to reproduce a correct diurnal cycle of HONO and NO_x, revealing this mechanism could be critical at night but not for daytime HONO and NO_x. Thus, it is not the important HONO formation pathway at CVAO. In the simulation "BaseCase + Nitro," the model performance is improved considerably, resulting in a noontime peak and comparable concentrations. The better performance of the model reveals the importance of dust in the photocatalytic conversions of nitrogen species to HONO and NO_x formation at CVAO.

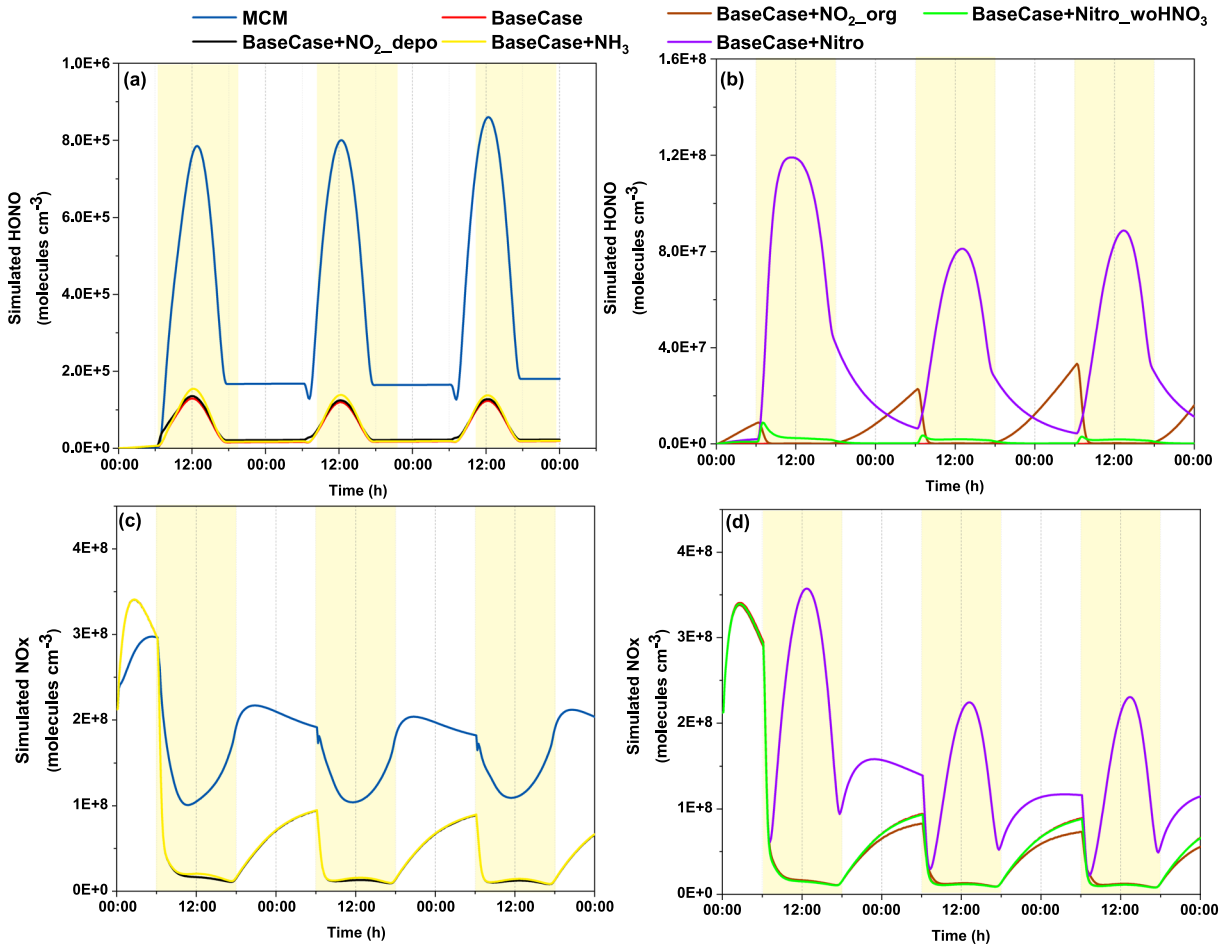

Figure 2. Modeled concentration of HONO (a and b) and NO_x (c + d) in different sensitivity tests. Blue line: "MCM" case. Red line: "BaseCase" case. Yellow line: "BaseCase + NH_3" case. Black line: "BaseCase + NO_2_depo" case. Orange line: "BaseCase + NO_2_org" case. Purple line: "BaseCase + Nitro" case. Green line: "BaseCase + Nitro_woHNO$_3$" case. The yellow shade is for the daytime modeling. Note that the simulated results are based on the air masses of Cluster 1.

Meanwhile, in the simulation "BaseCase + Nitro_woHNO$_3$," where the mechanism of photocatalytic conversion of gas-phase HNO_3 is set off, the modeled concentration and performance are sharply declined and inconsistent with the observations, highlighting the decisive role of photocatalytic HNO_3 conversion for HONO and NO_x formation. This result is consistent with the previous literature, which reported that the conceptual nitrate photolysis plays a critical role for remote NO_x and HONO concentrations (Reed et al., 2017; Ye et al., 2016). Overall, the illuminated mineral dust-carrying specific mineral oxides serve as an important reservoir for HONO and NO_x cycles in this remote marine tropical region, while the ocean seems not to be an important medium. Equally, it is suggested that the proposed HONO formation can be significant for other remote tropical regions that suffer from dust episodes. The applied uptake coefficient and ratios of BET-to-geometric surface can have an essential impact on the HONO and NO_x simulations. Thus, we have performed other sensitivity simulations in order to assess these impacts. The detailed results are given in Text S2 in Supporting Information S1.

3.2.2. HONO Simulation Analysis

The simulation "BaseCase + Nitro" successfully matches the HONO and NO_x diurnal cycles and concentrations from the simulated results. Thus, the applied mechanism is used for further simulations and analyses of the NO, NO_2, HONO, and O_3 patterns of the three clusters. The simulated and observed NO, NO_2, HONO, and O_3 patterns in simulation "BaseCase + Nitro" of Cluster 1 are compared and depicted in Figure 3. For the sake of clarity, the comparisons of the simulated and observed parameters in Cluster 2 and Cluster 3 are shown in Figures S5 and S6 in Supporting Information S1, respectively. Accordingly, we performed a correlation study. By means of hourly observational and simulated data, correlation coefficients (R) are calculated in order to evaluate the accuracy

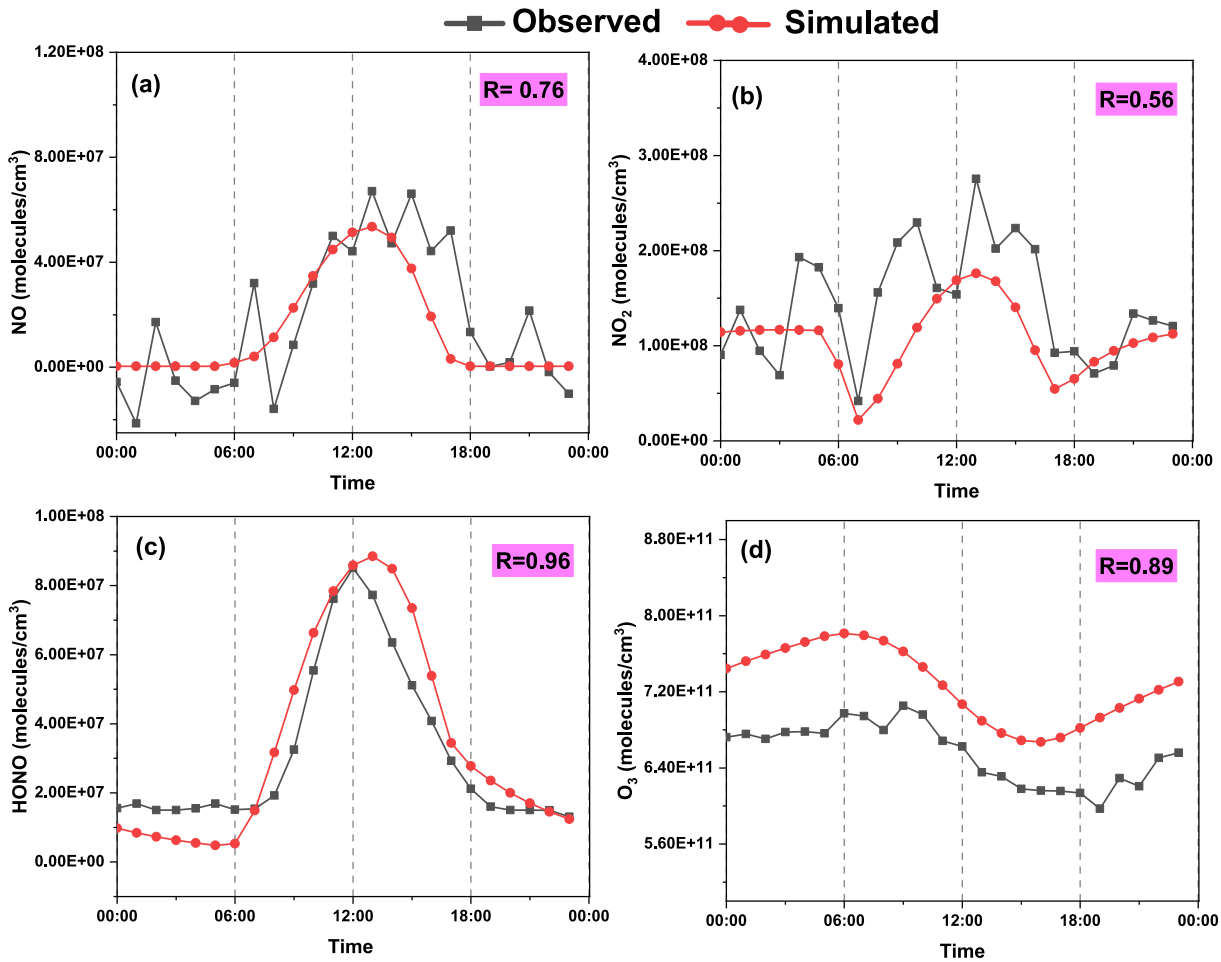

Figure 3. Comparison of simulated NO (a), NO_2 (b), HONO (c), and O_3 (d) concentration of Cluster 1 in the "BaseCase + Nitro" case with the observed levels at Cape Verde (CVAO). Note that the observed HONO value was obtained from Reed et al. (2017) and other observed species are measured from 2 October to 11 October 2017 during the MarParCloud campaign at CVAO. The comparison of simulated results of NO, NO_2, HONO, and O_3 in Clusters 2 and 3 are presented in Figures S5 and S6 in Supporting Information S1, respectively.

of the model results. The simulation "BaseCase + Nitro" for Cluster 1 reproduces well diurnal concentration profiles of HONO, NO, NO_2, and O_3 (see Figure 3) with high R values of 0.96, 0.76, 0.56, 0.89, respectively. For Clusters 2 and 3, high correlation coefficients are also calculated with values of 0.96 (0.96), 0.93 (0.83), and 0.89 (0.55) for HONO, NO, and O_3, respectively (see Figures S5 and S6 in Supporting Information S1). With R values of 0.34 and 0.27, the correlation for NO_2 is lower in these two clusters. Moreover, it can be seen that the implementation of nitrogen uptake mechanisms also offers a good model performance for pollutants, such as NO and O_3. This indicates that the mechanism involving photocatalytic conversions of RNS to HONO on the dust-surface together with the supporting data (i.e., emission data, initial data, and deposition rate of trace gases) is suitable, and can reasonably and intuitively reproduce the ambient atmospheric oxidation conditions during the MarParCloud campaign. Although the simulation can reproduce the diurnal pattern of HONO, NO, NO_2, and O_3, there is still discrepancy between modeled and measured NO_x and O_3. The discrepancy of modeled and measured NO_x concentrations could be explained by the uncertainty of emission rates of NO_x from the emission inventory. The comparisons of O_3 agree well for Clusters 1 and 2 (R = 0.89 and 0.89), but not for Cluster 3 (R = 0.55). This is due to the small contribution of Cluster 3 to the total observations, which included only 2 days (9 and 10 November). Also, the lack of available observational data for NO and NO_2 during the time period covering Cluster 3 could contribute to the low correlation coefficients (see Figure S6 in Supporting Information S1). The simulated concentrations of HNO_3 in the gas phase and NO_3^- in the particle phase are illustrated in Figure S7 in Supporting Information S1. The simulated HNO_3 (~5 pptv) was lower than the only published median value of HNO_3 at CVAO (~14 pptv) (Sander et al., 2013). In terms of pNO_3^-, the simulated NO_3^- concentration is around

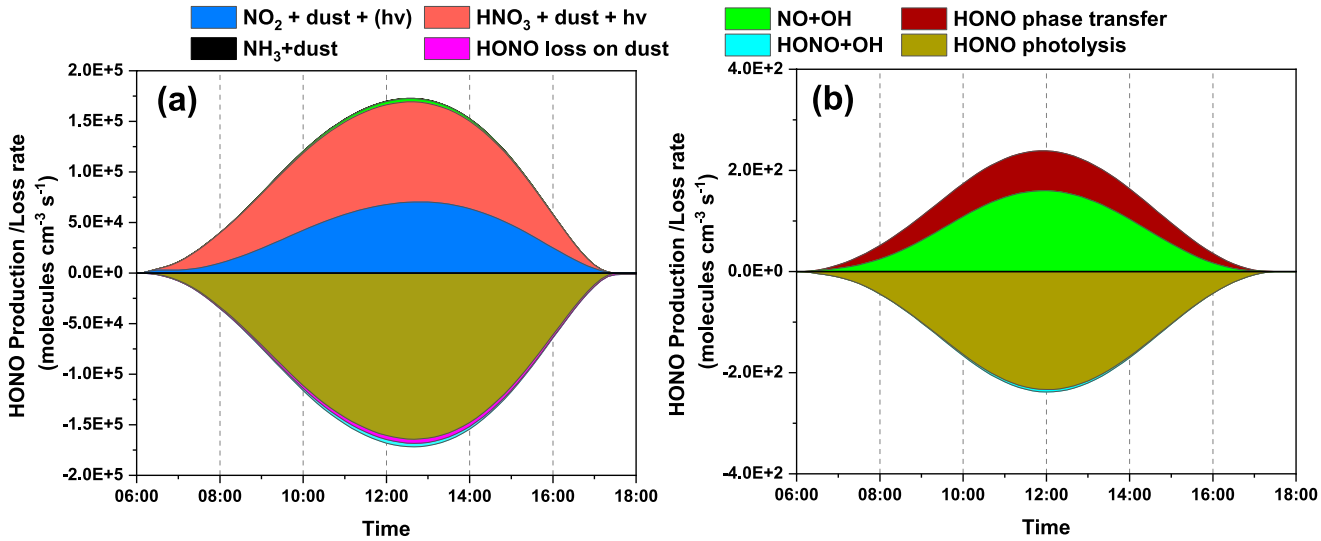

Figure 4. Modeled HONO production rates and loss rates of different chemical reactions in the "BaseCase + Nitro" case (a) and the "BaseCase" case (b). Note that these simulated results are based on the air masses of Cluster 1.

3.0 μg m^{-3}, which is greater than the observed NO_3^- concentration of PM_{10} (~1.5 μg m^{-3}). However, it should be noted that 1.5 μg m^{-3} NO_3^- was used to initialize the model. Without an initial NO_3^- concentration, it is plausible that a NO_3^- concentration within the measurement range would have been simulated.

Figure 4 shows the detailed HONO budget analysis of the simulations "BaseCase + Nitro" and "BaseCase" for Cluster 1. In the simulation "BaseCase," the primary sources are the gas-phase reaction of NO and OH with a maximum production rate of 1.6×10^2 molecules cm^{-3} s^{-1} at noon, followed by phase transfer (maximum rate of 7.9×10^1 molecules cm^{-3} s^{-1}, at noon) from the aqueous phase to the gas phase. When the mechanism of the dust-surface-photocatalytic conversions of RNS to HONO was considered (Figure 4a), HONO production rates were greatly enhanced with the dominant sources from photocatalytic HNO_3 conversion with a peak rate of 9.9×10^4 molecules cm^{-3} s^{-1}, which accounts for about 58% of total HONO production rate during noontime (11:00–14:00 local time). The second important HONO production pathway is the NO_2 reaction on dust (in the dark and in the sun), whose rate peaks at a value of 7.0×10^4 molecules cm^{-3} s^{-1}, contributing 40% of the total production rate. Other pathways, such as the gas reaction of NO an OH, HONO phase transfer and NH_3 absorbed on the dust, play a minor role in the HONO formation at CVAO. The major sink during daytime is HONO photolysis. The loss rates by HONO uptake on dust and reaction with OH have only a minor impact on the ambient HONO consumption at CVAO, with minor values of 4.0×10^3 and 3.3×10^3 molecules cm^{-3} s^{-1} during noontime. Overall, the rate analysis further emphasizes the critical role of mineral dust on HONO formation, especially due to dust-related photocatalysis of HNO_3/pNO_3^-.

3.2.3. Impact on HO_x

The comparison of simulated levels of OH and HO_2 are depicted in Figure S8 in Supporting Information S1. As we can see in this figure, three simulations showed the similar diurnal profiles of OH and HO_2 even in different air masses (clusters). The simulated OH (HO_2) concentration in Clusters 1, 2, and 3 are compared, with maximum values of 7.10 (3.61), 6.94 (3.47), and 7.13 (3.51) × 10^6 (10^8) molecules cm^{-3}. Similar profiles and levels were depicted between Cluster 1 and Clusters 2 and 3. It is reasonable to only use the simulated results of Cluster 1 for the following analysis. Figure 5 shows the simulated OH and HO_2 concentrations during the last day of the simulations "BaseCase + Nitro" and "BaseCase" of Cluster 1 and the comparison with measured OH and HO_2 levels during previous campaigns at CVAO. The simulated OH and HO_2 concentrations are comparable with previously measured levels (Vaughan et al., 2012), thus further illustrating the reasonable implementation of the model. When compared with other previous simulations, the simulated OH and HO_2 levels reasonably correspond with those reported by Whalley et al. (2010) in the summer of 2007 but are much lower than that simulated by Reed et al. (2017) in the autumn of 2015 at CVAO. It is noted that the box modeling by Whalley et al. (2010) used the MCM but was constrained by the hourly measured VOCs, O_3, and NO_x data and thus it is obvious that

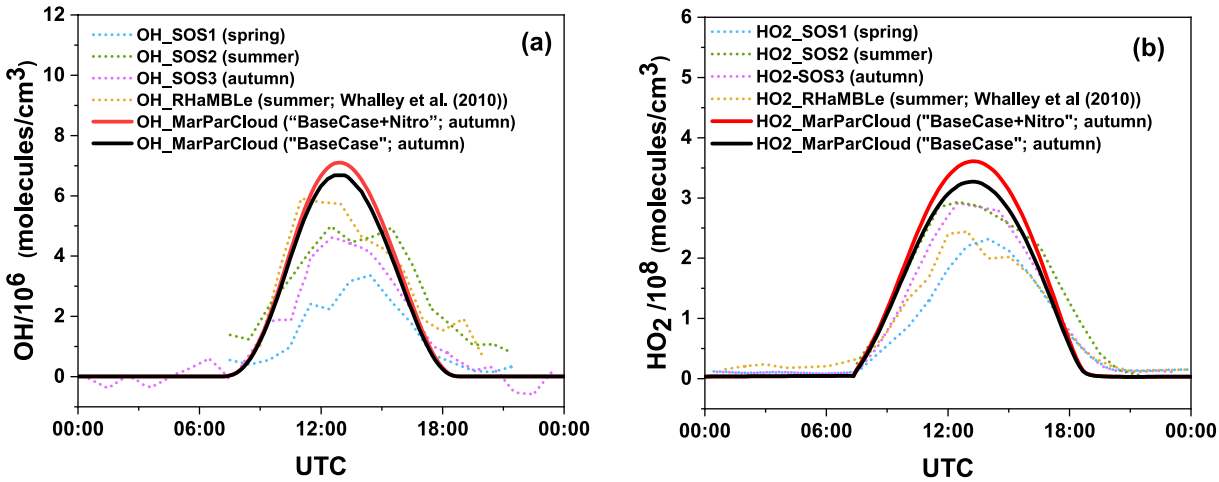

Figure 5. The simulated OH (a) and HO_2 (b) concentration during the last day of the simulation in "BaseCase + Nitro" and "BaseCase" case in comparison to measured concentration during other previous campaigns at Cape Verde (CVAO) (the OH and HO_2 level of SOS1, SOS2, SOS3, and RHaMBLe are obtained from Vaughan et al. (2012)).

the simulated OH and HO_2 levels were very similar to the ambient measured values. It is evident from the simulated diurnal cycles of OH and HO_2 shown in Figure 5 that the model independently, with/without coupling to the mechanisms of the dust, succeeds in calculating the OH and HO_2 behaviors at CVAO. The consideration of photocatalytic conversions of RNS on dust aerosol surfaces yielding HONO does not significantly change the HO_x levels even if the mixing ratio of HONO and NO_x at CVAO is increased. The largest contributions with about 6.5% (OH) and 10.0% (HO_2) are modeled during midday (9:00–16:00 LT), in line with the study of Reed et al. (2017). This supports the suggestion that HONO photolysis does not act as a key precursor of OH and thus also not significantly affect the HO_x budget in this remote MBL regime.

The detailed information of the statistical results of primary production rates and loss rates of OH and HO_2 radicals at CVAO for the simulation "BaseCase + Nitro" is documented in Table 2. Photolysis of O_3 presents the predominant primary OH source at CVAO. During the MarParCloud campaign, O_3 photolysis was the major source of OH in line with the simulations of Whalley et al. (2010), with a midday (9:00-16:00 LT) average production of 5.25×10^6 molecules cm^{-3} s^{-1} (74.6%). The recycling of HO_2 to OH by reacting with NO and O_3 followed, with an average proportion of 7.5%. Other sources are the H_2O_2 photolysis (3.74×10^5 molecules cm^{-3} s^{-1}; 5.3%), hypochlorous acid (HOCl) photolysis (3.70×10^5 molecules cm^{-3} s^{-1}; 5.3%), and hypoiodous acid (HOI) photolysis (2.40×10^5 molecules cm^{-3} s^{-1}; 3.4%), while HONO photolysis only accounted for a slight proportion of 1.8%, with a midday average production rate of 1.29×10^5 molecules cm^{-3} s^{-1} due to its low concentration at CVAO. Needless to say, the relative unimportant role of HONO photolysis on OH level at CVAO is completely different from that in the urban or polluted regions where HONO levels are in ppb range and its photolysis can contribute up to 60% of primary OH production during the daytime (Acker et al., 2006). For OH primary consumptions, the reaction of OH with CO represents the largest sink, with a fraction of 30.3% of the total sink rate during midday time, followed by CH_4 (27.1%), HCHO (12.0%), and CH_3OOH (8.1%). However, Whalley et al. (2010) also reported that CH_3CHO can act as an important sink for OH at CVAO resulting from the MCM box model constrained by observed VOCs data. The different role of CH_3CHO could be explained by Read et al. (2012), who reported a significant underestimation of simulated acetaldehyde compared to the observed values due to lack of an unknown oceanic flux of acetaldehyde in this region.

The production of HO_2 is dominated by the reaction of CO and OH, with a midday (9:00–16:00 LT) average production rate of 1.74×10^6 molecules cm^{-3} s^{-1}, accounting for about 32.0% of its production, followed by HCHO photolysis (7.68×10^5 molecules cm^{-3} s^{-1}; 14.2%), and the oxidation of HCHO by OH (6.87×10^5 molecules cm^{-3} s^{-1}; 12.7%) as also modeled by Whalley et al. (2010). Other pathways only play a minor role for HO_2 concentration. In comparison, the reactions of HO_2 and RO_2/HO_2 to form peroxides played a critical role in HO_2 consumption, with a fraction of 25.3% and 13.7% of the total loss rate at midday time, respectively. Other consumptions are the HO_2 uptake onto aerosols (12.9%), reaction with BrO (12.8%) and IO (12.0%), respectively.

Table 2
Summary of Major Primary Sources and Sinks of OH, HO_2 Radicals Simulated by MCM/CAPRAM Model in "BaseCase + Nitro" Case of Cluster 1

	Radical primary sources			Radical primary sinks		
Radical	P_{OH}/P_{HO_2}	Rate[a] (molecules cm^{-3} s^{-1})	Proportion (%)[b]	L_{OH}/L_{HO_2}	Rate [a] (molecules cm^{-3} s^{-1})	Proportion (%)[b]
OH radical	O_3 photolysis	5.25×10^6	74.6	CO	1.74×10^6	30.3
	$HO_2 + O_3$	4.23×10^5	6.0	CH_4	1.56×10^6	27.1
	H_2O_2 photolysis	3.74×10^5	5.3	HCHO	6.87×10^5	12.0
	HOCl photolysis	3.70×10^5	5.3	CH_3OOH	4.66×10^5	8.1
	HOI photolysis	2.40×10^5	3.4	H_2	4.48×10^5	7.8
	HONO photolysis	1.29×10^5	1.8	H_2O_2	2.68×10^5	4.7
	$HO_2 + NO$	1.09×10^5	1.5	O_3	2.68×10^5	4.7
	HOBr photolysis	7.96×10^4	1.1	HO_2	1.78×10^5	3.1
	CH_3OOH photolysis	6.80×10^4	1.0	CH_3CHO	1.31×10^5	2.3
HO_2 radical	$OH + CO$	1.74×10^6	32.0	CH_3O_2	1.21×10^6	25.3
	HCHO photolysis	7.68×10^5	14.2	HO_2	7.20×10^5	13.7
	HCHO + OH	6.87×10^5	12.7	HO_2 phase transfer	6.78×10^5	12.9
	$CH_3O + O_2$	5.93×10^5	10.9	BrO	6.71×10^5	12.8
	$OH + H_2$	4.48×10^5	8.3	IO	6.30×10^5	12.0
	$ClO + CH_3O_2$	3.79×10^5	7.0	O_3	4.24×10^5	8.1
	$OH + H_2O_2$	2.68×10^5	4.9	ClO	3.72×10^5	7.1
	$OH + O_3$	2.68×10^5	4.9	OH	1.79×10^5	3.4
	Cl + HCHO	1.52×10^5	2.8	$CH_3C(=O)O_2$	1.35×10^5	2.6
	Br + HCHO	1.25×10^5	2.3	CH_3O_2	1.18×10^5	2.3

[a]Rate is the midday (9:00–16:00 LT) average radical production/loss rate. [b]Proportion is the ratio of the target radical source/sink to the total quantified radical primary production/loss rates.

3.2.4. Interconnection Between RHS and HONO

To evaluate the impacts between RHS on RNS, a sensitivity test coupled with the dust-surface-photocatalytic conversions of RNS to HONO was conducted with and without the emission of I_2/Br_2 as constraints. The emission data of I_2 and Br_2 used in this simulation are used to obtain the typical daytime value of IO (1.5 pptv) and BrO (2.5 pptv) (Carpenter et al., 2010).

Figure 6 displays the comparison of the simulated HONO, NO_x, O_3, and XO (X = I, Br) from the simulated results constrained with and without I_2/Br_2 emission. It is clear that the simulated concentration of both HONO and NO_x declined when I_2 and Br_2 were emitted. The exact peaks of HONO and NO_x at midday appear earlier than expected when I_2 and Br_2 emissions were involved. The correlation coefficients of HONO and O_3 were slightly higher than without I_2/Br_2 emission, while the correlation coefficient of NO_x was a little lower. Furthermore, the modeled O_3 concentration was closer to the measurement without the I_2/Br_2 emission, indicating the important role of halogen chemistry for O_3 budget in pristine marine boundary layer. The reduced concentrations of NO_x and HONO were ascribed to the formation of bromine nitrate ($BrONO_2$), iodine nitrate ($IONO_2$) and organic nitrate ($RONO_2$) as well as HNO_3 through the reactions of NO_2 with OH and of NO with HO_2 (see the Reactions R11–R15), which are subsequently taken up by sea-spray aerosol. There, the hydrolysis of halogen nitrates to particulate nitrate suppresses NO_x recycling. Additionally, a loss of NO_2 at sunrise and sunset is simulated, which could be ascribed to the peak value of BrO. For the diurnal cycle of O_3, a lower O_3 concentration was displayed when the emission data of I_2 and Br_2 acted as constraints. Furthermore, a minor and narrow discrepancy between the maximum and minimum values of diurnal O_3 concentration profile was observed in the simulation without considering I_2 and Br_2 emission rates. The model presents a good performance for BrO and IO, which is in line with the observed ambient patterns at CVAO (see Carpenter et al., 2010 for details and Figure S9 in Supporting Information S1).

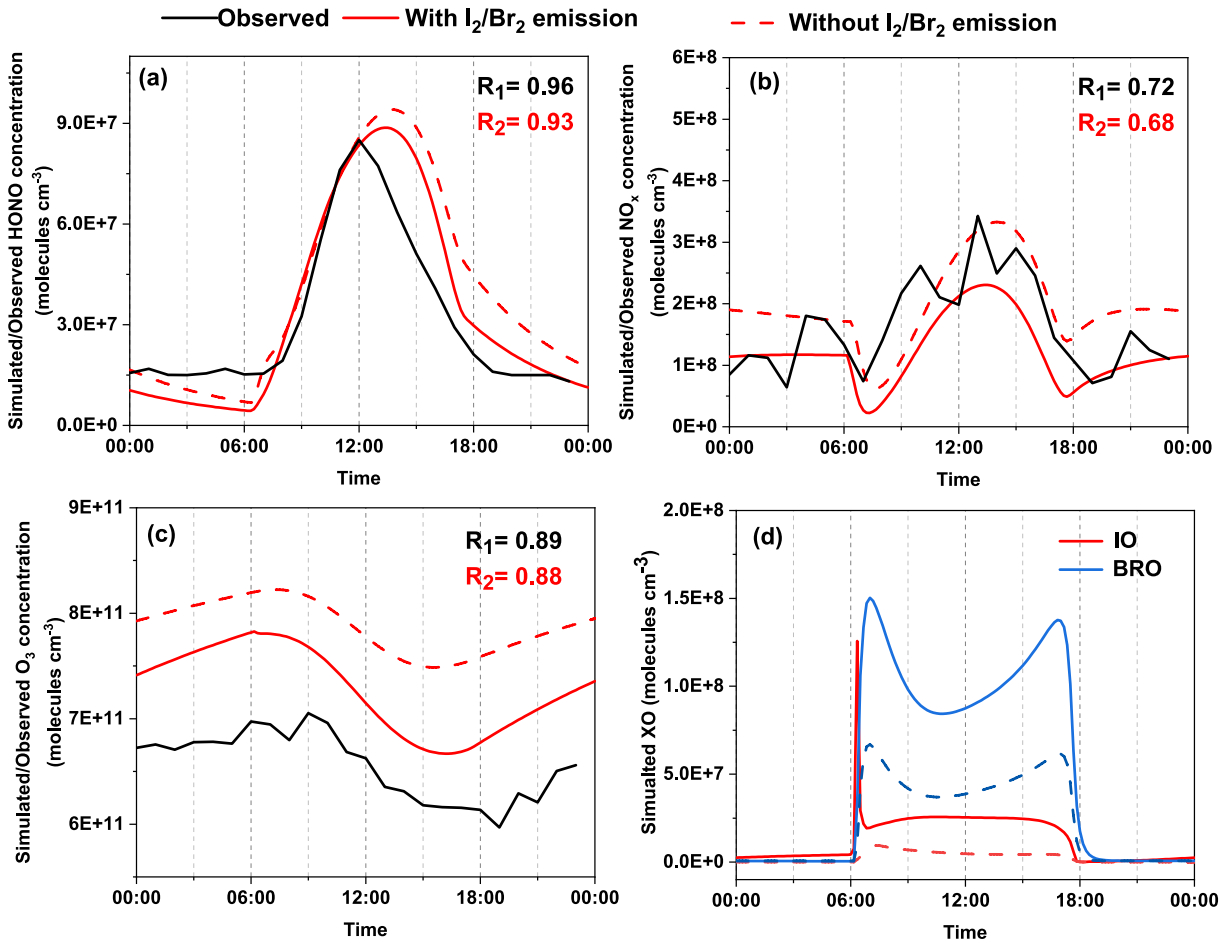

Figure 6. Simulated HONO (a), NO_x (b), O_3 (c), and XO (d) in "BaseCase + Nitro" case constrained with I_2/Br_2 emission data (red solid lines) and without I_2/Br_2 emission data (red dashed lines), and the observed value is the dark solid line. R_1 is the correlation coefficient between the observed with the simulated results constrained with I_2/Br_2 emission data and R_2 is the correlation coefficient between the observed with the simulated results without I_2/Br_2 emission data.

$$X_{2(gas)} \rightarrow X_{(gas)} + X_{(gas)} \ (X = \text{I or Br}) \quad \text{(R11)}$$

$$X_{(gas)} + O_{3(gas)} \rightarrow XO_{(gas)} \quad \text{(R12)}$$

$$XO_{(gas)} + NO_{2(gas)} \rightarrow XONO_{2(gas)} \quad \text{(R13)}$$

$$NO_{(gas)} + HO_{2(gas)} \rightarrow NO_{2(gas)} + OH_{(gas)} \quad \text{(R14)}$$

$$NO_{2\,(gas)} + OH_{(gas)} \rightarrow HNO_{3(gas)} \quad \text{(R15)}$$

4. Conclusion

The diurnal concentration trends, sources, and impacts on tropospheric oxidation chemistry of ambient HONO in the remote tropical MBL during the MarParCloud campaign were analyzed by conducting both field observations at CVAO and accompanied multiphase modeling. This study has identified the relative importance of different HONO formation mechanisms for the observed HONO and NO_x and highlighted the importance of photocatalytic conversions of RNS to HONO on mineral dust surfaces as well as the RHS chemistry on HONO/NO_x chemistry in the pristine tropical MBL. The inclusion of the photocatalytic conversions of RNS on mineral dust surfaces yielding to HONO significantly improved the multiphase model capability in simulating ambient concentrations of HONO, NO_x and other reactive pollutants (e.g., O_3, OH, HO_2, IO, and BrO). The model simulations

demonstrate a strong contribution from the photocatalytic HNO_3/pNO_3^- conversion on mineral dust, and elucidates the important role of dust aerosols for HONO formation, which is consistent with previous laboratory measurements. However, this dust-derived HONO source strongly depends on (a) the ratio of BET-to-geometric surface area and (b) the photocatalytic material content (i.e., on the photocatalytic dust properties), which could vary significantly under different environmental conditions. In contrast to polluted continental outflow regimes, the ocean-surface NO_2-to-HONO conversion mechanism cannot explain the observed HONO and NO_x values. The model performance constrained by the emission data of I_2/Br_2 has further improved the HONO and NO_x diurnal cycles by shifting the peaks toward noon. This indicates that the interaction of RHS and RNS can play an important role in the atmospheric chemistry of the MBL even under low NO_x conditions. Under the CVAO conditions, O_3 photolysis presents the primary source of the OH radical, and plays a major role in the HO_x radical chemistry. The photolysis of HONO only contributes slightly to the OH radical formation due to the very low HONO concentrations and the resulting small OH formation reaction rate. Overall, the present study provides a detailed understanding of HONO and NO_x chemistry in the pristine tropical MBL under the influence of dust particles and highlights the impacts of RHS chemistry on ambient HONO and NO_x levels. Finally, it is suggested that more efforts should be undertaken to better understand the particle-related HONO formation and its interplay with tropospheric RHS and RNS chemistry in the pristine MBL.

Conflict of Interest

The authors declare no conflicts of interest relevant to this study.

Data Availability Statement

The measurement data and model output of the present study can be accessed from Zenodo open data repository (https://doi.org/10.5281/zenodo.8070265), Jiang et al. (2023). The code of MCMv3.2 is provided via http://mcm.york.ac.uk (MCMv3.2, 2014) and CAPRAM code is available at https://capram.tropos.de/ (CAPRAM, 2021). The measurement data from the Cape Verde Atmospheric Observatory (CVAO) can be accessed via the EBAS home (https://ebas.nilu.no/) (EBAS Group, 2023). The trajectory data were obtained using the HYSPLIT model from NOAA Air Resources Laboratory (https://www.ready.noaa.gov/HYSPLIT_traj.php) (HYSPLIT, 2019).

Acknowledgments
We acknowledge the funding by the Leibniz Association SAW in the project "Marine biological production, organic aerosol particles and marine clouds: a Process Chain (MarParCloud)" (SAW-2016-TROPOS-2) and the Research and Innovation Staff Exchange EU project MARSU (69089). Moreover, we also received the funding support by the National Key Research and Development Program of China (2022YFC3701101) and the National Natural Science Foundation of China (42061160478). We also gratefully acknowledge the NOAA Air Resources Laboratory (ARL) for the provision of the HYSPLIT model used in this publication. We thank William Bloss and team for allowing the use of HONO data from Reed et al. (2017). We would like to thank Lucy Carpenter, James Lee, Katie Read, Shalini Punjabi, and Jim Hopkins at NCAS and WACL, University of York and Chris Reed at FAAM Airborne Laboratory, for the provision of all long-term data sets of NO_x, O_3, CO, etc. at CVAO. The authors also acknowledge the China Scholarship Council for supporting Ying Jiang to study at the Atmospheric Chemistry Department (ACD) of the Leibniz Institute for Tropospheric Research (TROPOS), Germany. Open Access funding enabled and organized by Projekt DEAL.

References

Acker, K., Möller, D., Wieprecht, W., Meixner, F., Berresheim, H., Gilge, S., et al. (2006). Strong daytime production of OH from HNO_2 at a rural mountain site. *Geophysical Research Letters*, *33*, L02809. https://doi.org/10.1029/2005GL024643

Adams, J., Rodriguez, D., & Cox, R. A. (2005). The uptake of SO_2 on Saharan dust: A flow tube study. *Atmospheric Chemistry and Physics*, *5*(10), 2679–2689. https://doi.org/10.5194/acp-5-2679-2005

Alfassi, Z., Huie, R., & Neta, P. (1986). Substituent effects on rates of one-electron oxidation of phenols by the radicals ClO_2, NO_2, and SO_3^-. *The Journal of Physical Chemistry*, *90*(17), 4156–4158. https://doi.org/10.1021/j100408a063

Alicke, B., Geyer, A., Hofzumahaus, A., Holland, F., Konrad, S., Pätz, H., et al. (2003). OH formation by HONO photolysis during the BERLIOZ experiment. *Journal of Geophysical Research*, *108*(D4), 8247. https://doi.org/10.1029/2001JD000579

Andersen, S., Carpenter, L., Nelson, B., Neves, L., Read, K., Reed, C., et al. (2021). Long-term NO_x measurements in the remote marine tropical troposphere. *Atmospheric Measurement Techniques*, *14*(4), 3071–3085. https://doi.org/10.5194/amt-14-3071-2021

Andersen, S., Carpenter, L., Reed, C., Lee, J., Chance, R., Sherwen, T., et al. (2023). Extensive field evidence for the release of HONO from the photolysis of nitrate aerosols. *Science Advances*, *9*(3), eadd6266. https://doi.org/10.1126/sciadv.add6266

Bräuer, P., Mouchel-Vallon, C., Tilgner, A., Mutzel, A., Böge, O., Rodigast, M., et al. (2019). Development of a protocol for the auto-generation of explicit aqueous-phase oxidation schemes of organic compounds. *Atmospheric Chemistry and Physics*, *19*(14), 9209–9239. https://doi.org/10.5194/acp-19-9209-2019

Calvert, J., Yarwood, G., & Dunker, A. (1994). An evaluation of the mechanism of nitrous acid formation in the urban atmosphere. *Research on Chemical Intermediates*, *20*(3), 463–502. https://doi.org/10.1163/156856794X00423

CAPRAM. (2021). Chemical aqueous phase mechanism (version 3.0) [Software]. Retrieved from https://capram.tropos.de/

Carpenter, L., Fleming, Z. L., Read, K., Lee, J., Moller, S., Hopkins, J., et al. (2010). Seasonal characteristics of tropical marine boundary layer air measured at the Cape Verde Atmospheric Observatory. *Journal of Atmospheric Chemistry*, *67*(2), 87–140. https://doi.org/10.1007/s10874-011-9206-1

Crilley, L. R., Kramer, L. J., Pope, F. D., Reed, C., Lee, J. D., Carpenter, L. J., et al. (2021). Is the ocean surface a source of nitrous acid (HONO) in the marine boundary layer? *Atmospheric Chemistry and Physics*, *21*(24), 18213–18225. https://doi.org/10.5194/acp-21-18213-2021

Cui, L., Li, R., Fu, H., Li, Q., Zhang, L., George, C., & Chen, J. (2019). Formation features of nitrous acid in the offshore area of the East China Sea. *Science of the Total Environment*, *682*, 138–150. https://doi.org/10.1016/j.scitotenv.2019.05.004

EBAS Group. (2023). EBAS home [Dataset]. Retrieved from https://ebas.nilu.no/

Ervens, B., George, C., Williams, J., Buxton, G., Salmon, G., Bydder, M., et al. (2003). CAPRAM 2.4 (MODAC mechanism): An extended and condensed tropospheric aqueous phase mechanism and its application. *Journal of Geophysical Research*, *108*(D14), 4426. https://doi.org/10.1029/2002JD002202

Fomba, K. W., Müller, K., van Pinxteren, D., Poulain, L., vanPinxteren, M., & Herrmann, H. (2014). Long-term chemical characterization of tropical and marine aerosols at the Cape Verde Atmospheric Observatory (CVAO) from 2007 to 2011. *Atmospheric Chemistry and Physics*, *14*(17), 8883–8904. https://doi.org/10.5194/acp-14-8883-2014

Forni, L. G., Mora-Arellano, V. O., Packer, J. E., & Willson, R. L. (1986). Nitrogen dioxide and related free radicals: Electron-transfer reactions with organic compounds in solutions containing nitrite or nitrate. *Journal of the Chemical Society, Perkin Transactions*, *2*(1), 1–6. https://doi.org/10.1039/P29860000001

George, C., Strekowski, R., Kleffmann, J., Stemmler, K., & Ammann, M. (2005). Photoenhanced uptake of gaseous NO_2 on solid organic compounds: A photochemical source of HONO? *Faraday Discussions*, *130*, 195–210. https://doi.org/10.1039/b417888m

Goldstein, S., Lind, J., & Merényi, G. (2005). Chemistry of peroxynitrites as compared to peroxynitrates. *Chemical Reviews*, *105*(6), 2457–2470. https://doi.org/10.1021/cr0307087

Gu, R., Zheng, P., Chen, T., Dong, C., Wang, Y., Liu, Y., et al. (2020). Atmospheric nitrous acid (HONO) at a rural coastal site in North China: Seasonal variations and effects of biomass burning. *Atmospheric Environment*, *229*, 117429. https://doi.org/10.1016/j.atmosenv.2020.117429

Guo, J., Tilgner, A., Yeung, C., Wang, Z., Louie, P., Luk, C., et al. (2014). Atmospheric peroxides in a polluted subtropical environment: Seasonal variation, sources and sinks, and importance of heterogeneous processes. *Environmental Science & Technology*, *48*(3), 1443–1450. https://doi.org/10.1021/es403229x

Heland, J., Kleffmann, J., Kurtenbach, R., & Wiesen, P. (2001). A new instrument to measure gaseous nitrous acid (HONO) in the atmosphere. *Environmental Science & Technology*, *35*(15), 3207–3212. https://doi.org/10.1021/es000303t

Hoffmann, E., Heinold, B., Kubin, A., Tegen, I., & Herrmann, H. (2021). The importance of the representation of DMS oxidation in global chemistry-climate simulations. *Geophysical Research Letters*, *48*(13), e2021GL094068. https://doi.org/10.1029/2021GL094068

Hoffmann, E., Tilgner, A., Schrödner, R., Bräuer, P., Wolke, R., & Herrmann, H. (2016). An advanced modeling study on the impacts and atmospheric implications of multiphase dimethyl sulfide chemistry. *Proceedings of the National Academy of Sciences of the United States of America*, *113*(42), 11776–11781. https://doi.org/10.1073/pnas.1606320113

Hoffmann, E., Tilgner, A., Wolke, R., Boge, O., Walter, A., & Herrmann, H. (2018). Oxidation of substituted aromatic hydrocarbons in the tropospheric aqueous phase: Kinetic mechanism development and modelling. *Physical Chemistry Chemical Physics*, *20*(16), 10960–10977. https://doi.org/10.1039/c7cp08576a

Hoffmann, E., Tilgner, A., Wolke, R., & Herrmann, H. (2019). Enhanced chlorine and bromine atom activation by hydrolysis of halogen nitrates from marine aerosols at polluted coastal areas. *Environmental Science & Technology*, *53*(2), 771–778. https://doi.org/10.1021/acs.est.8b05165

HYSPLIT. (2019). HYSPLIT Trajectory Model [Software]. Retrieved from https://www.ready.noaa.gov/HYSPLIT_traj.php

Jiang, Y., Hoffmann, E. H., Tilgner, A., & Herrmann, H. (2023). Insight into NOx and HONO chemistry in the tropical marine boundary layer at Cape Verde during MarParCloud campaign [Dataset]. Zenodo. https://doi.org/10.5281/zenodo.8070265

Jiang, Y., Xue, L., Gu, R., Jia, M., Zhang, Y., Wen, L., et al. (2020). Sources of nitrous acid (HONO) in the upper boundary layer and lower free troposphere of the NorthNorth China plain: Insights from the mount Tai observatory. *Atmospheric Chemistry and Physics*, *20*(20), 12115–12131. https://doi.org/10.5194/acp-20-12115-2020

Kebede, M., Scharko, N., Appelt, L., & Raff, J. (2013). Formation of nitrous ncid during nmmonia photooxidation on TiO_2 under atmospherically relevant conditions. *The Journal of Physical Chemistry Letters*, *4*(16), 2618–2623. https://doi.org/10.1021/jz401250k

Kebede, M., Varner, M., Scharko, N., Gerber, R., & Raff, J. (2013). Photooxidation of ammonia on TiO_2 as a source of NO and NO_2 under atmospheric conditions. *Journal of the American Chemical Society*, *135*(23), 8606–8615. https://doi.org/10.1021/ja401846x

Kohlmann, J., & Poppe, D. (1999). The tropospheric gas-phase degradation of NH_3 and its impact on the formation of N_2O and NO_x. *Journal of Atmospheric Chemistry*, *32*(3), 397–415. https://doi.org/10.1023/A:1006162910279

Lamarque, J.-F., Bond, T. C., Eyring, V., Granier, C., Heil, A., Klimont, Z., et al. (2010). Historical (1850–2000) gridded anthropogenic and biomass burning emissions of reactive gases and aerosols: Methodology and application. *Atmospheric Chemistry and Physics*, *10*(15), 7017–7039. https://doi.org/10.5194/acp-10-7017-2010

Li, D., Xue, L., Wen, L., Wang, X., Chen, T., Mellouki, A., et al. (2018). Characteristics and sources of nitrous acid in an urban atmosphere of northern China: Results from 1-yr continuous observations. *Atmospheric Environment*, *182*, 296–306. https://doi.org/10.1016/j.atmosenv.2018.03.033

Liu, Y., Lu, K., Li, X., Dong, H., Tan, Z., Wang, H., et al. (2019). A comprehensive model test of the HONO sources constrained to field measurements at rural North China Plain. *Environmental Science & Technology*, *53*(7), 3517–3525. https://doi.org/10.1021/acs.est.8b06367

Liu, Z., Wang, Y., Costabile, F., Amoroso, A., Zhao, C., Huey, L., et al. (2014). Evidence of aerosols as a media for rapid daytime HONO production over China. *Environmental Science & Technology*, *48*(24), 14386–14391. https://doi.org/10.1021/es504163z

Loughner, C., Tzortziou, M., Shroder, S., & Pickering, K. (2016). Enhanced dry deposition of nitrogen pollution near coastlines: A case study covering the Chesapeake Bay estuary and Atlantic Ocean coastline. *Journal of Geophysical Research*, *121*, 14221–14238. https://doi.org/10.1002/2016JD025571

MCMv3.2. (2014). Master Chemical Mechanism (version 3.2) [Software]. Retrieved from http://mcm.york.ac.uk

Ndour, M., Conchon, P., D'Anna, B., Ka, O., & George, C. (2009). Photochemistry of mineral dust surface as a potential atmospheric renoxification process. *Geophysical Research Letters*, *36*, L05816. https://doi.org/10.1029/2008GL036662

Ndour, M., D'Anna, B., George, C., Ka, O., Balkanski, Y., Kleffmann, J., et al. (2008). Photoenhanced uptake of NO_2 on mineral dust: Laboratory experiments and model simulations. *Geophysical Research Letters*, *35*, L05812. https://doi.org/10.1029/2007GL032006

Pai, S., Heald, C., & Murphy, J. (2021). Exploring the global importance of atmospheric ammonia oxidation. *ACS Earth and Space Chemistry*, *5*(7), 1674–1685. https://doi.org/10.1021/acsearthspacechem.1c00021

Park, J., & Lee, Y. (1988). Solubility and decomposition kinetics of nitrous acid in aqueous solution. *The Journal of Physical Chemistry*, *92*(22), 6294–6302. https://doi.org/10.1021/j100333a025

Read, K., Carpenter, L., Arnold, S., Beale, R., Nightingale, P., Hopkins, J., et al. (2012). Multiannual observations of acetone, methanol, and acetaldehyde in remote tropical Atlantic air: Implications for atmospheric OVOC budgets and oxidative capacity. *Environmental Science & Technology*, *46*(20), 11028–11039. https://doi.org/10.1021/es302082p

Reed, C., Evans, M. J., Crilley, L. R., Bloss, W. J., Sherwen, T., Read, K. A., et al. (2017). Evidence for renoxification in the tropical marine boundary layer. *Atmospheric Chemistry and Physics*, *17*(6), 4081–4092. https://doi.org/10.5194/acp-17-4081-2017

Ren, Y., Stieger, B., Spindler, G., Grosselin, B., Mellouki, A., Tuch, T., et al. (2020). Role of the dew water on the ground surface in HONO distribution: A case measurement in Melpitz. *Atmospheric Chemistry and Physics*, *20*(21), 13069–13089. https://doi.org/10.5194/acp-20-13069-2020

Ridley, B. A., & Grahek, F. E. (1990). A small, low flow, high sensitivity reaction vessel for NO chemiluminescence detectors. *Journal of Atmospheric and Oceanic Technology*, *7*, 301–311. https://doi.org/10.1175/1520-0426(1990)007<0307:ASLFHS>2.0.CO;2

Saliba, N., Yang, H., & Finlayson-Pitts, B. (2001). Reaction of gaseous nitric oxide with nitric acid on silica surfaces in the presence of water at room temperature. *The Journal of Physical Chemistry A*, *105*(45), 10339–10346. https://doi.org/10.1021/jp012330r

Salvador, P., Almeida, S., Cardoso, J., Almeida-Silva, M., Nunes, T., Cerqueira, M., et al. (2016). Composition and origin of PM_{10} in Cape Verde: Characterization of long-range transport episodes. *Atmospheric Environment*, *127*, 326–339. https://doi.org/10.1016/j.atmosenv.2015.12.057

Sander, R., Pszenny, P., Keene, C., Crete, E., Deegan, B., Long, S., et al. (2013). Gas phase acid, ammonia and aerosol ionic and trace element concentrations at Cape Verde during the Reactive Halogens in the Marine Boundary Layer (RHaMBLe) 2007 intensive sampling period. *Earth System Science Data*, *5*(2), 385–392. https://doi.org/10.5194/essd-5-385-2013

Sehili, A., Wolke, R., Knoth, O., Simmel, M., Tilgner, A., & Herrmann, H. (2005). Comparison of different model approaches for the simulation of multiphase processes. *Atmospheric Environment*, *39*(23/24), 4403–4417. https://doi.org/10.1016/j.atmosenv.2005.02.039

Sherwen, T., Evans, M. J., Carpenter, L. J., Andrews, S. J., Lidster, R. T., Dix, B., et al. (2016). Iodine's impact on tropospheric oxidants: A global model study in GEOS-Chem. *Atmospheric Chemistry and Physics*, *16*(2), 1161–1186. https://doi.org/10.5194/acp-16-1161-2016

Spataro, F., & Ianniello, A. (2014). Sources of atmospheric nitrous acid: State of the science, current research needs, and future prospects. *Journal of the Air & Waste Management Association*, *64*(11), 1232–1250. https://doi.org/10.1080/10962247.2014.952846

Stemmler, K., Ammann, M., Donders, C., Kleffmann, J., & George, C. (2006). Photosensitized reduction of nitrogen dioxide on humic acid as a source of nitrous acid. *Nature*, *440*(7081), 195–198. https://doi.org/10.1038/nature04603

Stone, D., Whalley, L., & Heard, D. (2012). Tropospheric OH and HO_2 radicals: Field measurements and model comparisons. *Chemical Society Reviews*, *41*(19), 6348–6404. https://doi.org/10.1039/C2CS35140D

Su, H., Cheng, Y., Oswald, R., Behrendt, T., Trebs, I., Meixner, F., et al. (2011). Soil nitrite as a source of atmospheric HONO and OH radicals. *Science*, *333*(6049), 1616–1618. https://doi.org/10.1126/science.1242266

Tang, M., Huang, X., Lu, K., Ge, M., Li, Y., Cheng, P., et al. (2017). Heterogeneous reactions of mineral dust aerosol: Implications for tropospheric oxidation capacity. *Atmospheric Chemistry and Physics*, *17*(19), 11727–11777. https://doi.org/10.5194/acp-17-11727-2017

VandenBoer, T., Brown, S., Murphy, J., Keene, W., Young, C., Pszenny, A., et al. (2013). Understanding the role of the ground surface in HONO vertical structure: High resolution vertical profiles during NACHTt 11. *Journal of Geophysical Research*, *118*, 10155–10171. https://doi.org/10.1002/jgrd.50721

van Pinxteren, M., Fomba, K. W., Triesch, N., Stolle, C., Wurl, O., Bahlmann, E., et al. (2020). Marine organic matter in the remote environment of the Cape Verde islands–an introduction and overview to the MarParCloud campaign. *Atmospheric Chemistry and Physics*, *20*(11), 6921–6951. https://doi.org/10.5194/acp-20-6921-2020

Vaughan, S., Ingham, T., Whalley, L. K., Stone, D., Evans, M. J., Read, K. A., et al. (2012). Seasonal observations of OH and HO_2 in the remote tropical marine boundary layer. *Atmospheric Chemistry and Physics*, *12*(4), 2149–2172. https://doi.org/10.5194/acp-12-2149-2012

Villena, G., Wiesen, P., Cantrell, C., Flocke, F., Fried, A., Hall, S., et al. (2011). Nitrous acid (HONO) during polar spring in Barrow, Alaska: A net source of OH radicals? *Journal of Geophysical Research*, *116*, D00R07. https://doi.org/10.1029/2011JD016643

Wang, X., Dalton, E., Payne, Z., Perrier, S., Riva, M., Raff, J., & George, C. (2020). Superoxide and nitrous acid production from nitrate photolysis is enhanced by dissolved aliphatic organic matter. *Environmental Science and Technology Letters*, *8*(1), 53–58. https://doi.org/10.1021/acs.estlett.0c00806

Weinzierl, B., Sauer, D., Esselborn, M., Petzold, A., Veira, A., Rose, M., et al. (2011). Microphysical and optical properties of dust and tropical biomass burning aerosol layers in the Cape Verde region—An overview of the airborne in situ and lidar measurements during SAMUM-2. *Tellus B: Chemical and Physical Meteorology*, *63*(4), 589–618. https://doi.org/10.1111/j.1600-0889.2011.00566.x

Wen, L., Chen, T., Zheng, P., Wu, L., Wang, X., Mellouki, A., et al. (2019). Nitrous acid in marine boundary layer over eastern Bohai Sea, China: Characteristics, sources, and implications. *Science of the Total Environment*, *670*, 282–291. https://doi.org/10.1016/j.scitotenv.2019.03.225

Whalley, L. K., Furneaux, K. L., Goddard, A., Lee, J. D., Mahajan, A., Oetjen, H., et al. (2010). The chemistry of OH and HO_2 radicals in the boundary layer over the tropical Atlantic Ocean. *Atmospheric Chemistry and Physics*, *10*(4), 1555–1576. https://doi.org/10.5194/acp-10-1555-2010

Wolke, R., Sehili, A. M., Simmel, M., Knoth, O., Tilgner, A., & Herrmann, H. (2005). Spaccim: A parcel model with detailed microphysics and complex multiphase chemistry. *Atmospheric Environment*, *39*(23/24), 4375–4388. https://doi.org/10.1016/j.atmosenv.2005.02.038

Wong, K. W., Oh, H.-J., Lefer, B. L., Rappenglück, B., & Stutz, J. (2011). Vertical profiles of nitrous acid in the nocturnal urban atmosphere of Houston, TX. *Atmospheric Chemistry and Physics*, *11*(8), 3595–3609. https://doi.org/10.5194/acp-11-3595-2011

Wong, K. W., Tsai, C., Lefer, B., Haman, C., Grossberg, N., Brune, W. H., et al. (2012). Daytime HONO vertical gradients during SHARP 2009 in Houston, TX. *Atmospheric Chemistry and Physics*, *12*(2), 635–652. https://doi.org/10.5194/acp-12-635-2012

Xue, C., Ye, C., Kleffmann, J., Zhang, W., He, X., Liu, P., et al. (2022). Atmospheric measurements at Mt. Tai – Part II: HONO budget and radical ($RO_x + NO_3$) chemistry in the lower boundary layer. *Atmospheric Chemistry and Physics*, *22*(2), 1035–1057. https://doi.org/10.5194/acp-22-1035-2022

Yang, J., Shen, H., Guo, M., Zhao, M., Jiang, Y., Chen, T., et al. (2021). Strong marine-derived nitrous acid (HONO) production observed in the coastal atmosphere of northern China. *Atmospheric Environment*, *244*, 117948. https://doi.org/10.1016/j.atmosenv.2020.117948

Ye, C., Chen, H., Hoffmann, E., Mettke, P., Tilgner, A., He, L., et al. (2021). Particle-phase photoreactions of HULIS and TMIs establish a strong source of H_2O_2 and particulate sulfate in the winter North China Plain. *Environmental Science & Technology*, *55*(12), 7818–7830. https://doi.org/10.1021/acs.est.1c00561

Ye, C., Heard, D., & Whalley, L. (2017). Evaluation of novel routes for NO_x formation in remote regions. *Environmental Science & Technology*, *51*(13), 7442–7449. https://doi.org/10.1021/acs.est.6b06441

Ye, C., Zhang, N., Gao, H., & Zhou, X. (2017). Photolysis of particulate nitrate as a source of HONO and NO_x. *Environmental Science & Technology*, *51*(12), 6849–6856. https://doi.org/10.1021/acs.est.7b00387

Ye, C., Zhou, X., Pu, D., Stutz, J., Festa, J., Spolaor, M., et al. (2016). Rapid cycling of reactive nitrogen in the marine boundary layer. *Nature*, *532*(7600), 489–491. https://doi.org/10.1038/nature17195

Zha, Q., Xue, L., Wang, T., Xu, Z., Yeung, C., Louie, P., & Luk, C. (2014). Large conversion rates of NO_2 to HNO_2 observed in air masses from the South China Sea: Evidence of strong production at sea surface? *Geophysical Research Letters*, *41*, 7710–7715. https://doi.org/10.1002/2014GL061429

Zhang, R., Gen, M., Huang, D., Li, Y., & Chan, C. (2020). Enhanced sulfate production by nitrate photolysis in the presence of halide ions in atmospheric particles. *Environmental Science & Technology*, *54*(7), 3831–3839. https://doi.org/10.1021/acs.est.9b06445

Zhou, X., Zhang, N., TerAvest, M., Tang, D., Hou, J., Bertman, S., et al. (2011). Nitric acid photolysis on forest canopy surface as a source for tropospheric nitrous acid. *Nature Geoscience*, *4*(7), 440–443. https://doi.org/10.1038/ngeo1164

Zhu, Y., Tilgner, A., Hoffmann, E., Herrmann, H., Kawamura, K., Yang, L., et al. (2020). Multiphase MCM–CAPRAM modeling of the formation and processing of secondary aerosol constituents observed during the Mt. Tai summer campaign in 2014. *Atmospheric Chemistry and Physics*, *20*(11), 6725–6747. https://doi.org/10.5194/acp-20-6725-2020

References From the Supporting Information

Adams, J. W., Rodriguez, D., & Cox, R. (2005). The uptake of SO_2 on Saharan dust: A flow tube study. *Atmospheric Chemistry and Physics*, *5*(10), 2679–2689. https://doi.org/10.5194/acp-5-2679-2005

Andrews, S. J. (2013). *Short-lived halocarbon species in the oceans and atmosphere (PhD thesis)*. University of York.

Andersen, S., Carpenter, L., Reed, C., Lee, C., Chance, R., Sherwen, T., et al. (2023). Extensive field evidence for the release of HONO from the photolysis of nitrate aerosols. *Science Advances*, *9*(3), eadd6266. https://doi.org/10.1126/sciadv.add6266

Beale, R., Dixon, J., Arnold, S., Liss, P., & Nightingale, P. (2013). Methanol, acetaldehyde, and acetone in the surface waters of the Atlantic Ocean. *Journal of Geophysical Research: Oceans*, *118*(10), 5412–5425. https://doi.org/10.1002/jgrc.20322

Booge, D., Marandino, C., Schlundt, C., Palmer, P., Schlundt, M., Atlas, E., et al. (2016). Can simple models predict large-scale surface ocean isoprene concentrations? *Atmospheric Chemistry and Physics*, *16*(18), 11807–11821. https://doi.org/10.5194/acp-16-11807-2016

Bräuer, P., Tilgner, A., Wolke, R., & Herrmann, H. (2013). Mechanism development and modelling of tropospheric multiphase halogen chemistry: The CAPRAM Halogen Module 2.0 (HM2). *Journal of Atmospheric Chemistry*, *70*(1), 19–52. https://doi.org/10.1007/s10874-013-9249-6

Broadgate, W. J., Liss, P., & Penkett, S. (1997). Seasonal emissions of isoprene and other reactive hydrocarbon gases from the ocean. *Geophysical Research Letters*, *24*(21), 2675–2678. https://doi.org/10.1029/97GL02736

Cahill, T. M. (2014). Ambient acrolein concentrations in coastal, remote, and urban regions in California. *Environmental Science & Technology*, *48*(15), 8507–8513. https://doi.org/10.1021/es5014533

Carpenter, L., Fleming, Z., Read, K., Lee, J., Moller, S., Hopkins, J., et al. (2010). Seasonal characteristics of tropical marine boundary layer air measured at the Cape Verde Atmospheric Observatory. *Journal of Atmospheric Chemistry*, *67*(2–3), 87–140. https://doi.org/10.1007/s10874-011-9206-1

Crowley, J., Ammann, M., Cox, R., Hynes, R., Jenkin, M., Mellouki, A., et al. (2010). Evaluated kinetic and photochemical data for atmospheric chemistry: Volume V - Heterogeneous reactions on solid substrates. *Atmospheric Chemistry and Physics*, *10*(18), 9059–9223. https://doi.org/10.5194/acp-10-9059-2010

Debevec, C., Sauvage, S., Gros, V., Salameh, T., Sciare, J., Dulac, F., & Locoge, N. (2021). Seasonal variation and origins of volatile organic compounds observed during 2 years at a western Mediterranean remote background site (Ersa, Cape Corsica). *Atmospheric Chemistry and Physics*, *21*(3), 1449–1484. https://doi.org/10.5194/acp-21-1449-2021

El Zein, A., & Bedjanian, Y. (2012). Reactive uptake of HONO to TiO_2 surface: "dark" reaction. *The Journal of Physical Chemistry A*, *116*(14), 3665–3672. https://doi.org/10.1021/jp300859w

El Zein, A., Romanias, M., & Bedjanian, Y. (2013). Kinetics and products of heterogeneous reaction of HONO with Fe_2O_3 and Arizona Test Dust. *Environmental Science & Technology*, *47*(12), 6325–6331. https://doi.org/10.1021/es400794c

Hackenberg, S., Andrews, S., Airs, R., Arnold, S., Bouman, H., Cummings, D., et al. (2017). Basin-Scale observations of monoterpenes in the Arctic and Atlantic oceans. *Environmental Science & Technology*, *51*(18), 10449–10458. https://doi.org/10.1021/acs.est.7b02240

Hanisch, F., & Crowley, J. (2001). The heterogeneous reactivity of gaseous nitric acid on authentic mineral dust samples, and on individual mineral and clay mineral components. *Physical Chemistry Chemical Physics*, *3*(12), 2474–2482. https://doi.org/10.1039/B101700O

Hepach, H., Quack, B., Raimund, S., Fischer, T., Atlas, E., & Bracher, A. (2015). Halocarbon emissions and sources in the equatorial Atlantic Cold Tongue. *Biogeosciences*, *12*(21), 6369–6387. https://doi.org/10.5194/bg-12-6369-2015

Huang, L., Zhao, Y., Li, H., & Chen, Z. (2015). Kinetics of heterogeneous reaction of sulfur dioxide on authentic mineral dust: Effects of relative humidity and hydrogen peroxide. *Environmental Science & Technology*, *49*(18), 10797–10805. https://doi.org/10.1021/acs.est.5b03930

Jones, C., Hornsby, K., Sommariva, R., Dunk, R., Von Glasow, R., McFiggans, G., & Carpenter, L. (2010). Quantifying the contribution of marine organic gases to atmospheric iodine. *Geophysical Research Letters*, *37*, L18804. https://doi.org/10.1029/2010GL043990

Karagulian, F., & Rossi, M. (2005). The heterogeneous chemical kinetics of NO_3 on atmospheric mineral dust surrogates. *Physical Chemistry Chemical Physics*, *7*(17), 3150–3162. https://doi.org/10.1039/B506750M

Karagulian, F., Santschi, C., & Rossi, M. (2006). The heterogeneous chemical kinetics of N_2O_5 on $CaCO_3$ and other atmospheric mineral dust surrogates. *Atmospheric Chemistry and Physics*, *6*(5), 1373–1388. https://doi.org/10.5194/acp-6-1373-2006

Kebede, M., Scharko, N., Appelt, L., & Raff, J. (2013). Formation of nitrous acid during ammonia photooxidation on TiO_2 under atmospherically relevant conditions. *The Journal of Physical Chemistry Letters*, *4*(16), 2618–2623. https://doi.org/10.1021/jz401250k

Kleffmann, J., Becker, K., & Wiesen, P. (1998). Heterogeneous NO_2 conversion processes on acid surfaces: Possible atmospheric implications. *Atmospheric Environment*, *32*(16), 2721–2729. https://doi.org/10.1016/S1352-2310(98)00065-X

Kohlmann, J.-P., & Poppe, D. (1999). The tropospheric gas-phase degradation of NH_3 and its impact on the formation of N_2O and NO_x. *Journal of Atmospheric Chemistry*, *32*(3), 397–415. https://doi.org/10.1023/A:1006162910279

Kolusu, S., Schlünzen, K., Grawe, D., & Seifert, R. (2017). Chloromethane and dichloromethane in the tropical Atlantic Ocean. *Atmospheric Environment*, *150*, 417–424. https://doi.org/10.1016/j.atmosenv.2016.11.037

Loughner, P., Tzortziou, M., Shroder, S., & Pickering, K. (2016). Enhanced dry deposition of nitrogen pollution near coastlines: A case study covering the Chesapeake Bay estuary and Atlantic Ocean coastline. *Journal of Geophysical Research*, *121*, 14221–14238. https://doi.org/10.1002/2016JD025571

Lowe, D., Topping, D., & McFiggans, G. (2009). Modelling multi-phase halogen chemistry in the remote marine boundary layer: Investigation of the influence of aerosol size resolution on predicted gas and condensed-phase chemistry. *Atmospheric Chemistry and Physics*, *9*(14), 4559–4573. https://doi.org/10.5194/acp-9-4559-2009

Pai, S., Heald, C., & Murphy, J. (2021). Exploring the global importance of atmospheric ammonia oxidation. *ACS Earth and Space Chemistry*, *5*(7), 1674–1685. https://doi.org/10.1021/acsearthspacechem.1c00021

Plass, C., Koppmann, R., & Rudolph, J. (1992). Light hydrocarbons in the surface water of the mid-Atlantic. *Journal of Atmospheric Chemistry*, *15*(3–4), 235–251. https://doi.org/10.1007/BF00115396

Read, K., Carpenter, L., Arnold, S., Beale, R., Nightingale, P., Hopkins, J., et al. (2012). Multiannual observations of acetone, methanol, and acetaldehyde in remote tropical Atlantic air: Implications for atmospheric OVOC budgets and oxidative capacity. *Environmental Science & Technology*, *46*(20), 11028–11039. https://doi.org/10.1021/es302082p

Read, K. A., Mahajan, A. S., Carpenter, L. J., Evans, M. J., Faria, B. V., Heard, D. E., et al. (2008). Extensive halogen-mediated ozone destruction over the tropical Atlantic Ocean. *Nature*, *453*(7199), 1232–1235. https://doi.org/10.1038/nature07035

Reed, C., Evans, M. J., Crilley, L. R., Bloss, W. J., Sherwen, T., Read, K. A., et al. (2017). Evidence for renoxification in the tropical marine boundary layer. *Atmospheric Chemistry and Physics*, *17*(6), 4081–4092. https://doi.org/10.5194/acp-17-4081-2017

Saiz-Lopez, A., Fernandez, R., Ordóñez, C., Kinnison, D., Gómez Martín, J., Lamarque, J.-F., & Tilmes, S. (2014). Iodine chemistry in the troposphere and its effect on ozone. *Atmospheric Chemistry and Physics*, *14*(23), 13119–13143. https://doi.org/10.5194/acp-14-13119-2014

Sander, R., Pszenny, A., Keene, W., Crete, E., Deegan, B., Long, M., et al. (2013). Gas phase acid, ammonia and aerosol ionic and trace element concentrations at Cape Verde during the Reactive Halogens in the Marine Boundary Layer (RHaMBLe) 2007 intensive sampling period. *Earth System Science Data*, *5*(2), 385–392. https://doi.org/10.5194/essd-5-385-2013

Seifert, R., Delling, N., Richnow, H., Kempe, S., Hefter, J., & Michaelis, W. (1999). Ethylene and methane in the upper water column of the subtropical Atlantic. *Biogeochemistry*, *44*(1), 73–91. https://doi.org/10.1007/BF00992999

Seisel, S., Börensen, C., Vogt, R., & Zellner, R. (2004). The heterogeneous reaction of HNO_3 on mineral dust and γ-alumina surfaces: A combined Knudsen cell and DRIFTS study. *Physical Chemistry Chemical Physics*, *6*(24), 5498–5508. https://doi.org/10.1039/B410793D

Singh, H., Chen, Y., Staudt, A., Jacob, D., Blake, D., Heikes, B., & Snow, J. (2001). Evidence from the Pacific troposphere for large global sources of oxygenated organic compounds. *Nature*, *410*(6832), 1078–1081. https://doi.org/10.1038/35074067

Singh, H., Salas, L., Chatfield, R., Czech, E., Fried, A., Walega, J., et al. (2004). Analysis of the atmospheric distribution, sources, and sinks of oxygenated volatile organic chemicals based on measurements over the Pacific during TRACE-P. *Journal of Geophysical Research*, *109*, D15S07. https://doi.org/10.1029/2003JD003883

Singh, H., Tabazadeh, A., Evans, M., Field, B., Jacob, D., Sachse, G., et al. (2003). Oxygenated volatile organic chemicals in the oceans: Inferences and implications based on atmospheric observations and air-sea exchange models. *Geophysical Research Letters*, *30*(16), 1862. https://doi.org/10.1029/2003GL017933

Stemmler, K., Ndour, M., Elshorbany, Y., Kleffmann, J., D'anna, B., George, C., et al. (2007). Light induced conversion of nitrogen dioxide into nitrous acid on submicron humic acid aerosol. *Atmospheric Chemistry and Physics*, *7*(16), 4237–4248. https://doi.org/10.5194/acp-7-4237-2007

Stubbins, A., Uher, G., Law, C., Mopper, K., Robinson, C., & Upstill-Goddard, R. (2006). Open-ocean carbon monoxide photoproduction. *Deep Sea Research Part II: Topical Studies in Oceanography*, *53*(14–16), 1695–1705. https://doi.org/10.1016/j.dsr2.2006.05.011

Tang, M., Thieser, J., Schuster, G., & Crowley, J. (2010). Uptake of NO_3 and N_2O_5 to Saharan dust, ambient urban aerosol and soot: A relative rate study. *Atmospheric Chemistry and Physics*, *10*(6), 2965–2974. https://doi.org/10.5194/acp-10-2965-2010

Tang, M., Thieser, J., Schuster, G., & Crowley, J. (2012). Kinetics and mechanism of the heterogeneous reaction of N_2O_5 with mineral dust particles. *Physical Chemistry Chemical Physics*, *14*(24), 8551–8561. https://doi.org/10.1039/C2CP40805H

Ullerstam, M., Vogt, R., Langer, S., & Ljungstrom, E. (2002). The kinetics and mechanism of SO_2 oxidation by O_3 on mineral dust. *Physical Chemistry Chemical Physics*, *4*(19), 4694–4699. https://doi.org/10.1039/b203529b

Villena, G., Wiesen, P., Cantrell, C., Flocke, F., Fried, A., Hall, S., et al. (2011). Nitrous acid (HONO) during polar spring in Barrow, Alaska: A net source of OH radicals? *Journal of Geophysical Research*, *116*, D00R07. https://doi.org/10.1029/2011JD016643

Vlasenko, A., Sjogren, S., Weingartner, E., Stemmler, K., Gäggeler, H., & Ammann, M. (2006). Effect of humidity on nitric acid uptake to mineral dust aerosol particles. *Atmospheric Chemistry and Physics*, *6*(8), 2147–2160. https://doi.org/10.5194/acp-6-2147-2006

von Kuhlmann, R. (2001). Tropospheric photochemistry of ozone, its precursors and the hydroxyl radical: A 3D-modeling study considering non-methane hydrocarbons (PhD thesis).

Wagner, C., Hanisch, F., Holmes, N., Coninck, H., Schuster, G., & Crowley, J. (2008). The interaction of N_2O_5 with mineral dust: Aerosol flow tube and Knudsen reactor studies. *Atmospheric Chemistry and Physics*, *8*(1), 91–109. https://doi.org/10.5194/acp-8-91-2008

Wohl, C., Brown, I., Kitidis, V., Jones, A., Sturges, W., Nightingale, P., & Yang, M. (2020). Underway seawater and atmospheric measurements of volatile organic compounds in the Southern Ocean. *Biogeosciences*, *17*(9), 2593–2619. https://doi.org/10.5194/bg-17-2593-2020

Wong, K., Oh, H.-J., Lefer, B., Rappenglück, B., & Stutz, J. (2011). Vertical profiles of nitrous acid in the nocturnal urban atmosphere of Houston, TX. *Atmospheric Chemistry and Physics*, *11*(8), 3595–3609. https://doi.org/10.5194/acp-11-3595-2011

Wong, K., Tsai, C., Lefer, B., Grossberg, N., & Stutz, J. (2013). Modeling of daytime HONO vertical gradients during SHARP 2009. *Atmospheric Chemistry and Physics*, *13*(7), 3587–3601. https://doi.org/10.5194/acp-13-3587-2013

Xiao, X., Prinn, R., Fraser, P., Simmonds, P., Weiss, R., O'Doherty, S., et al. (2010). Optimal estimation of the surface fluxes of methyl chloride using a 3-D global chemical transport model. *Atmospheric Chemistry and Physics*, *10*(12), 5515–5533. https://doi.org/10.5194/acp-10-5515-2010

Yang, M., Beale, R., Liss, P., Johnson, M., Blomquist, B., & Nightingale, P. (2014). Air–sea fluxes of oxygenated volatile organic compounds across the Atlantic Ocean. *Atmospheric Chemistry and Physics*, *14*, 7499–7517. https://doi.org/10.5194/acp-14-7499-2014

Ye, C., Heard, D. E., & Whalley, L. K. (2017). Evaluation of novel routes for NO_x formation in remote regions. *Environmental Science & Technology*, *51*(13), 7442–7449. https://doi.org/10.1021/acs.est.6b06441

Zhou, X., & Mopper, K. (1990). Apparent partition coefficients of 15 carbonyl compounds between air and seawater and between air and freshwater; implications for air-sea exchange. *Environmental Science & Technology*, *24*(12), 1864–1869. https://doi.org/10.1021/es00082a013